

EIDESSTATTLICHE ERKLÄRUNG

Ich erkläre an Eides statt, dass ich die vorliegende Arbeit selbstständig verfasst, andere als die angegebenen Quellen/Hilfsmittel nicht benutzt, und die den benutzten Quellen wörtlich und inhaltlich entnommenen Stellen als solche kenntlich gemacht habe. Das in TUGRAZonline hochgeladene Textdokument ist mit der vorliegenden Dissertation identisch.

Datum

Unterschrift

For something to exist, it has to be observed. For something to exist, it has to have a position in time and space. And this explains why nine-tenths of the mass of the universe is unaccounted for. Nine-tenths of the universe is the knowledge of the position and direction of everything in the other tenth.

Every atom has its biography, every star its file, every chemical exchange its equivalent of the inspector with a clipboard. It is unaccounted for because it is doing the accounting for the rest of it, and you cannot see the back of your own head. Nine-tenths of the universe, in fact, is the paperwork.

Thief of Time by Terry Pratchett

Preface

The transfer of small particles such as electrons, protons or even hydrogen atoms is a very fundamental process that occurs in chemical transformations throughout all fields. Especially in complex biological systems a multitude of parallel and consecutive transfer steps is coupled to different chemical reactions e.g. in the respiratory chain. In order to understand these complex systems on a fundamental level insights into the basic physics of all these individual steps are necessary.

This thesis is dedicated to five different scientific questions about the simplest type of transfer process: the so-called degenerate self-exchange. The focus is on kinetics since these are the main requirement for mechanistic interpretations. Theoretically and experimentally the concept of self-exchange is well established in the context of Marcus theory for either electrons or protons alone. Rather recently it was expanded to coupled processes and hydrogen atoms as well. The first chapter will summarize the theoretical background and recent developments.

Since degenerate self-exchange is an isoenergetic process most conventional methods are not suitable. One of the few methods that circumvent this problem is dynamic ESR spectroscopy which is the main experimental technique in this work. It uses the nuclear spin configuration as marker to distinguish chemically identical species. Chapter two will give an introduction in the relevant aspects and limitations of this method.

For the experimental section there are three studies on degenerate electron self-exchange and two on hydrogen atom transfer. The applicability of the concept of outer sphere reorganization from Marcus theory is demonstrated for the electron self-exchange of zinc tetraphenylporphyrine and the corresponding radical cation in chapter three.

Chapter four summarizes the preliminary investigations on a new experimental routine that we developed especially to study activated processes in ionic liquids. Upon using binary mixtures the temperature dependence of viscosity which biases thermodynamic data could be minimized. In order to demonstrate the applicability tetrathiafulvalene and its corresponding radical cation were used as probe.

Chapter five contains the first study of electron self-exchange kinetics for 9H-thioxanthen-9-one 10,10-dioxide and its corresponding radical anion. The goal was to switch between electron and proton-coupled electron self-exchange with the pH-value, however, we encountered rapid reversible dimerization.

In chapter six the first successful ESR line-broadening experiment for a hydrogen atom transfer is presented. The kinetics of the phthalimide-N-oxyl radical and the neutral N-hydroxyphthalimide revealed a dependence on the medium's dynamic viscosity in a series of organic solvents.

Finally chapter seven concludes with a study on dimers of the blue aroxyl and the corresponding phenol. The temperature dependence of the spectra revealed an alternating line-width effect for a rapid hydrogen atom motion. The reaction pathway, experimental thermodynamic parameters and tunnelling contributions were confirmed conclusively by quantum-chemical calculations.

Vorwort

In allen Disziplinen der Chemie spielt die Übertragung von einzelnen Teilchen wie Elektronen, Protonen oder sogar Wasserstoffatomen eine wichtige Rolle als einer von wenigen fundamentalen Teilschritten aus denen sich chemische Reaktionen zusammensetzen. Gerade in komplexen biologischen Systemen ist oft eine Vielzahl aufeinander folgender und/oder paralleler Übertragungen dieser Art zu beobachten. Als Beispiel soll die Atmungskette genannt werden. Um nun solche Systeme in ihrer Gesamtheit zu verstehen, ist es notwendig die physikalischen Grundlagen jedes Teilschrittes beschreiben zu können.

Die vorliegende Arbeit beschäftigt sich mit fünf unterschiedlichen wissenschaftlichen Fragestellungen um den einfachsten Typ von Übertragungsreaktionen: dem sogenannten Selbstaustausch. Der Fokus liegt auf der Kinetik solcher Prozesse, da dies die Grundlage für jede weitere mechanistische Interpretation ist. Für die Übertragung eines einzelnen Elektrons oder eines Protons sind die experimentellen Methoden und Theorien – im speziellen die sogenannte Marcus Theorie – bereits gut etabliert. Ziel in der aktuellen Forschung ist es, diese auch auf gekoppelte Mechanismen zu übertragen. Die theoretischen Grundlagen sowie relevante Entwicklungen werden in Kapitel eins behandelt.

Da Selbstaustausch per Definition ein isoenergetischer Prozess ist, versagen die meisten konventionellen experimentellen Methoden. Dynamische ESR Spektroskopie, die hauptsächlich für diese Arbeit verwendet wurde, ist eine der wenigen anwendbaren Methoden, da sie chemisch äquivalente Moleküle anhand ihrer Kernspinkonfiguration unterscheiden kann. In Kapitel zwei werden die relevanten Aspekte und Limitierungen der Methode erläutert.

Der experimentelle Teil gliedert sich in drei Projekte zum Thema Elektronenselbstaustausch und zwei zum Thema Wasserstoffatomselbstaustausch. In Kapitel drei wird die Anwendbarkeit des Konzepts der Lösungsmittelreorganisation für den Elektronenselbstaustausch von Zink-Tetraphenylporphyrin und dem entsprechenden Radikal Kation demonstriert.

Kapitel vier beschreibt die Voruntersuchungen, die im Weiteren zur Entwicklung einer neuen Methode geführt haben, welche speziell für die Untersuchung von aktivierten Prozessen in

ionischen Flüssigkeiten geeignet ist. Dabei sollte der störende Einfluss auf die experimentellen Aktivierungsparameter, der von der stark temperaturabhängigen Viskosität kommt, minimiert werden. Die prinzipielle Anwendbarkeit wurde am System Tetrathiafulvalen und dem entsprechenden Radikal Kation erfolgreich gezeigt.

Bei dem Projekt in Kapitel fünf handelt es sich um eine kurze Studie zum Elektronenselbstaustausch zwischen 9H-thioxanthen-9-on 10,10-dioxid und dem entsprechenden Radikal Anion. Es wurde zudem versucht, über den pH-Wertes den Mechanismus vom einfachen Elektronenselbstaustausch zu einem gekoppelten Prozess umzuschalten. Eine schnelle reversible Dimerisierung macht dies jedoch nicht möglich.

Im sechsten Kapitel wird vom ersten erfolgreichen ESR-Linienverbreiterungselement für Wasserstoffatomselbstaustausch berichtet. Das untersuchte System ist das Phtalimid-N-oyl Radikal mit dem entsprechenden N-Hydroxyphtalimid. In einer Serie verschiedener Lösungsmittel wurde eine Abhängigkeit von der Viskosität für diese Kinetik festgestellt.

Das letzte Kapitel beschäftigt sich mit Dimeren des blauen Aroxyls und dem entsprechenden Phenol. Ein alternierender Linienbreiteneffekt wurde in temperaturabhängigen Studien festgestellt, der von einer schnellen Bewegung des Wasserstoffatoms im Komplex kommt. Der generelle Reaktionsmechanismus, die experimentellen Aktivierungsbarrieren und Tunnelbeiträge konnten mit quantenchemischen Rechnungen bestätigt werden.

Acknowledgements

During the three years of my PhD studies I had the pleasure to meet many people who contributed in various ways. Some were directly involved in the scientific work itself, others inspired ideas or helped to maintain all the equipment. Further there were those who kept me motivated when I needed it. In the following I explicitly want to thank...

Günter Grampp my supervisor who did not only offer opportunity and environment for this thesis but also a lot of freedom to choose the direction of the research by myself. Moreover, all the insightful advice and discussions helped a lot in the interpretation and/or understanding of the results.

Stephan Landgraf who did not only offer advice and inspired some of the work directly but also provided, explained and maintained all the necessary equipment for solvent characterization. Further I'm grateful that I was kept involved in teaching master students in the framework of his lab courses.

Anne-Marie Kelterer who taught about, helped with and actually did a lot of the quantum chemical calculations within the final project of this thesis.

Marijana Marković who did a great part of the quantum chemical calculations and took many nice photos while climbing.

Kenneth Rasmussen - my mentor and friend - who (unfortunately) went away to explore current issues on the final frontier of mankind in the early stages of my time as PhD student. Live long and prosper!

Boryana Mladenova-Kattnig for all the nice conversations in our shared office and the patient help with experiments and simulations even after her contract expired. I wish you and your family all the best in the UK.

Hilde Freißmuth who constantly reminded me about safety in the lab and put a lot of work in the purification of all the required chemicals together with her apprentice Ines Gössler. I hope that both of you will enjoy your new future challenges.

Helmut Eisenkölbl who utilized the Eisen-effect a lot which solves most hard and software problems by his mere presence. Enjoy your retirement!

Herbert Lang who helped me in reviving the electrochemical setup and the construction of the “Kübl” that eliminated freezing problems at the temperature control unit.

Marion Hofmeister who basically runs the administration our institute by herself. Without your help I´d probably lost myself in the crazy jungle of university administration.

My students Martin Berghold (Master Thesis), Freskida Goni (Project Assistant) and Pia Riedl (Bachelor Thesis) who contributed more than just the experimental work since I really enjoy tutoring. I´m grateful as well that all of you endured my slightly chaotic style...

Further there is a long list of fellow PhD students who made my working days fun by discussions about almost everything. First of all I´d like to thank Yen Ha Thi Hai for all the great discussions, the endless supply of Vietnamese lunches and introducing me to Darja. I also had a lot of nice conversations with my office buddy Hao Hoang Minh and his wife Van Thi Bich Pham who did not only their thesis here but also started their family during this time. Then there were the fellow ESR guys – Beate Sudy and Patcharanan Choto – who additionally had a lot of patience with sharing equipment. The last in chronological order was Alexander Wankmüller with whom I discovered to have quite some hobbies in common.

Besides the fellow students I also enjoyed the company of a few postdocs. I´m very grateful to Troung Nguyen Xuan who stopped by in Graz every year to have a lot of fun at work until he even enabled my visit to Vietnam. Finally I really enjoyed to collaborate with Aep Patah who inspired my interest in electro chemistry again.

Apart from work I´m really grateful for my patient and loving Darja who was and is sharing all the ups and downs of life with me. Soon we´ll both end this chapter of our life together and proceed into our shared future in the real world of adulthood.

Then there is my family in Vorarlberg and in Burgenland who always believed in me, offered advice and support and a place to retreat to whenever I needed it.

Moreover, there is a large number of friends who joined my numerous adventures in the mountains of Austria as well as fictional places such as the continent of Aventurien or the state of Rokugan just to name a few.

Finally I´d like to thank the Austrian Science Fond (FWF) who enabled me to pay my bills during this time in the framework of the EU-ERANET project I 931-N19.

Inhaltsverzeichnis

1. Theory of Electron and Proton Coupled Electron Transfer	3
1.1 Introduction	3
1.2 Transition State Theory	4
1.3 Assumptions and Predictions of Marcus Theory on ET	6
1.4 Concept and Study of Reorganization	8
1.5 The Preexponential Factor	11
1.6 Application to PCET	13
1.7 References	15
2. ESR Spectroscopy	17
2.1 Introduction	17
2.2 Fundamentals of Magnetic Resonance	18
2.3 Technological Considerations	20
2.4 The static ESR Spectrum	21
2.5 Dynamic ESR	24
2.6 Application to Self-Exchange Processes	31
2.7 ENDOR	33
2.8 References	36
3. Methods and Instruments	37
3.1 Solvent Purification.....	37
3.2 Sample Preparation	37
3.3 Spectrometer Setup.....	38
3.4 The Flow System	39
3.5 The Electrochemical Setup	40
3.6 The Photochemical Setup	42
3.6 Density and Viscosity	43
4. Electron Self-Exchange of ZnTPP and its corresponding π-Radical Cation.....	44
4.1 Introduction	44
4.2 Experimental.....	45
4.3 Results and Discussion.....	46
4.4 Outlook and Conclusion.....	48
4.5 References	49

5. Electron Self-Exchange of TTF/TTF^{•+} in a Binary Mixture of Ionic Liquids	50
5.1 Introduction	50
5.2 Theoretical Considerations	51
5.3 Experimental	53
5.4 Results and Discussion	54
5.5 Conclusion and Outlook	55
5.6 References	56
6. Electron self-exchange of 9H-thioxanthen-9-one 10,10-dioxide and its corresponding radical anion	57
6.1 Introduction	57
6.2 Experimental	58
6.3 Results and Discussion	58
6.4 Outlook and Conclusion	60
6.5 References	61
7. Hydrogen atom self-exchange of NHPI/PINO	62
7.1 Introduction	62
7.2 Experimental	63
7.3 Results and Discussion	63
7.4 Outlook and Conclusion	67
7.5 References	68
8. Hydrogen atom transfer dynamics in a hydrogen bonded complex of the Blue Aroxyl and the corresponding Phenol	69
8.1 Introduction	69
8.2 Experimental	70
8.3 Results and Discussion	71
8.4 Conclusion	73
8.5 References	73

1. Theory of Electron and Proton Coupled Electron Transfer

1.1 Introduction

In a very fundamental approach every chemical reaction can be broken down into simple elementary steps. These occur either consecutive or parallel and are abundant throughout all chemical transformations. Upon these elementary steps electron transfer (ET) is one of the simplest since chemical bonds are neither broken nor formed. This is the most significant difference to proton transfer (PT) and proton coupled electron transfer (PCET) even though the theoretical description works rather similar.

There is a large and diverse list of chemical disciplines where these processes are currently of interest. Large industries around electronics or hydrocarbon oxidation e.g. utilize the related chemistry in a huge scale. In technological science the most obvious field is the technology of energy transformation and storage. Examples are batteries, accumulators and fuel cells [1.1] as well as photovoltaic cells. [1.2] The latter subject is closely related to its biochemical equivalent in photosynthesis. [1.3] From the manifold biological aspects especially the chemistry of DNA where these transfer processes occur in various functions seems noteworthy. [1.4] Another growing field is the so-called organo catalysis which might substitute expensive rare metals in future. [1.5] Despite the diversity of applications and scientific interests the fundamental theory, however, is quite universal.

Historically the theoretical approach presented in this thesis originates in the late 1940ies after the Second World War. Since ET is usually a fast process close to the limits of diffusion the limited time resolution of experimental techniques made its kinetics inaccessible. The newly developed in methods using radioactive tracers, optical polarimetry and magnetic resonance of this time, however, overcame these problems.

The increasing amount of experimental data enabled a rapid development in the field of theory which finally resulted in the formulation of Marcus theory in 1956 [1.6] which was rewarded the Nobel Prize in 1992. The circumstances that lead to this scientific breakthrough are elaborated in his Nobel lecture. [1.7] Up to now this theory has been continuously tested, improved and further expanded to different types of ET and related processes such as PT and PCET.

Since this thesis focuses on homogeneous processes in solution only relevant aspects of the theory are discussed. For ET there is a growing selection of textbooks [1.8] which are supplemented by a multitude of review articles [1.9] on various aspects of Marcus theory. For the more recent developments in the field of PCET the literature is more recent. [1.10]

1.2 Transition State Theory

Since Marcus theory was formulated within the framework of the transition state theory (TST) from Eyring [1.11] it is necessary for the further discussion to introduce its basic concepts. It is still the standard approach in the theoretical description of chemical kinetics, however, details about its assumptions and limitations are rarely discussed in basic chemical literature. The main idea is that chemical reactions undergo a smooth continuous transformation of all reactant coordinates during the reaction. This transformation crosses a so-called transition state (TS) or activated complex that corresponds to a saddle point on the corresponding potential energy surface. In the nomenclature of chemical equations a bimolecular process can thus be expressed by equation 1.1 where A and D denote the reactants.



Since the theory assumes an equilibrium in between reactants and TS – this approximation is strictly speaking not valid for the usually large differences in energy of these states. The corresponding equilibrium constant K is displayed in equation 1.2. In the following square brackets will be used to symbolize the concentration of a species.

$$K = \frac{[TS]}{[A][D]} \quad (1.2)$$

The corresponding rate r is expressed by equation 1.3. Here k denotes the chemical rate constant and ν the frequency of crossing the TS.

$$r = k [A][D] = \nu [TS] \quad (1.3)$$

Combining equations 1.2 and 1.3 the rate constant k can be formulated as displayed in equation 1.4.

$$k = \nu K \quad (1.4)$$

In the context of statistical mechanics the thermodynamic equilibrium constant is defined by equation 1.5. Here Q_i is the molecular partition function for the i^{th} reactant at standard conditions, ΔE_0 the energy difference of reactants and products in the ground state in molar energies, k_B the Boltzmann constant and T the absolute temperature in K.

$$K = \prod Q_i e^{-\frac{\Delta E_0}{k_B T}} \quad (1.5)$$

The partition function refers to all electronic, nuclear, translational, vibrational and rotational contributions of the reactant and is obtained from the sum over all energy levels j as given in equation 1.6. Here $g_{i,j}$ is introduced for degenerate energy states with the same energy $E_{i,j}$.

$$Q_i = Q_{el} Q_{nuc} Q_{trans} Q_{vib} Q_{rot} = \sum_j g_{i,j} e^{-\frac{E_{i,j}}{k_B T}} \quad (1.6)$$

Inserting equation 1.5 in equation 1.2 yields equation 1.7 where V^0 denotes the molar volume at standard conditions.

$$K = \frac{Q_{TS}}{Q_A Q_D} V^0 e^{-\frac{\Delta E_0}{k_B T}} \quad (1.7)$$

In order to obtain a general expression for the reaction rate the partition function of vibration will now be separated since only vibrational fluctuations are assumed to advance the reaction coordinate. For small values of x the approximation that $e^{-x} \approx 1-x$ is valid. Thus the partition function of vibration can be written according to equation 1.8. Here k_B denotes the Boltzmann constant, T the absolute temperature, h the Planck constant and ν the frequency of vibration.

$$Q_{vib} = \frac{1}{1 - e^{-\frac{h\nu}{k_B T}}} \approx \frac{k_B T}{h\nu} \quad (1.8)$$

In equation 1.9 a simplified equilibrium constant K' is presented. It is derived from equation 1.7 where the partition functions were separated in Q_{vib} and the remaining contributions Q'_{TS} . Additionally Q_{vib} is approximated as shown in equation 1.8.

$$K' = \frac{k_B T}{h\nu} \frac{Q'_{TS}}{Q_A Q_D} V^0 e^{-\frac{\Delta E_0}{k_B T}} \quad (1.9)$$

Inserting equation 1.9 in the general definition of the rate constant in equation 1.4 gives the final description of k in equation 1.10.

$$k = \frac{k_B T}{h} \frac{Q'_{TS}}{Q_A Q_D} V^0 e^{-\frac{\Delta E_0}{k_B T}} \quad (1.10)$$

Even though empirical data proved this theory to be considerably accurate for many reactions with the limitation that neither tunnelling through the barrier nor the possibility to cross the TS multiple times is given. The so called electronic transmission factor κ_{el} was therefore introduced as displayed in equation 1.10. This factor characterizes the probability of TS to go to the product state. For most reactions it is usually close or equal to unity, however, if nuclear tunnelling plays a role it increases to larger values.

$$k = \frac{k_B T}{h} \kappa_{el} \frac{Q'_{TS}}{Q_A Q_D} V^0 e^{-\frac{\Delta E_0}{k_B T}} \quad (1.11)$$

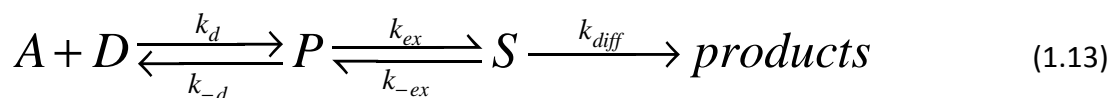
Experimentalists usually use the simplified Arrhenius equation 1.12 instead of equation 1.11 since partition functions are not observable quantities. A denotes the preexponential factor and ΔG^* the activation barrier which are obtained as intercept and slope of a plot of $\ln(k)$ versus T^{-1} .

$$k = A e^{-\frac{\Delta G^*}{k_B T}} \quad (1.12)$$

1.3 Assumptions and Predictions of Marcus Theory on ET

The most peculiar assumption with Marcus theory is the application of the Franck-Condon Principle. This principle originated in the field of absorption spectroscopy where every excitation is predicted to be vertical due to the fact that the electron moves significantly faster than the nuclei. In the field of quantum chemistry the Born-Oppenheimer approximation uses the same argument to separate nuclear and electronic wave functions to speed up calculations. In Marcus theory this argument is expanded to a chemical reaction where the electron jumps forth and back in-between two states until one of them reaches a configuration that stabilizes the electron. Chapter 2.4 discusses this in detail.

Marcus expanded the reaction scheme of the standard TST in equation 1.1 to the one displayed in equation 1.13. The TS is now positioned between two distinguishable complexes: The precursor complex P refers to the reactants in close contact and the successor complex S to the products in close contact respectively. Close contact stands for a reaction distance equal to the sum of the reactants radii.



In this mechanism the first and the third step – association and dissociation – are related to simple mass transport in order to bring the reactants in and out of close contact. Both processes are well established in the field of physical chemistry. [1.11] Note that these processes also depend strongly of the reactants charge since electrostatic interaction might occur. In this work all systems contained either two uncharged or only one charged reactant in order to eliminate this additional effect. The corresponding kinetics of this reaction scheme are discussed in chapter 2.4 whereas here the focus is on the thermodynamic aspects.

So the actual Marcus theory deals with the second step that transfers the system from P to S . The resonance splitting V_{ps} accounts for the electronic interaction of reactants and products

respectively. Further the reaction is assumed to proceed by vibrational changes without breaking chemical bonds so that both states can sufficiently be described by the harmonic oscillator approximation. With this assumptions the reaction can be drawn as two parabolas in a two-dimensional cut-out of the potential energy surface as displayed in figure 1-1. There λ denotes the so-called reorganization energy, ΔG° the driving force which is the difference in the energetic minima of the parabolas and ΔG^* the activation barrier required to reach the actual TS.

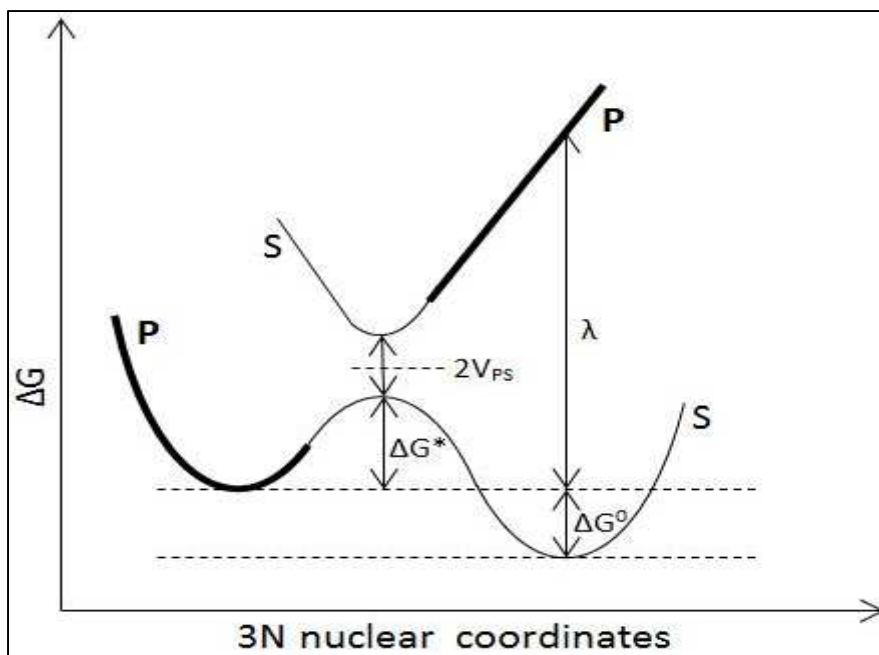


Figure 1-1: Two dimensional cut-out from the potential energy surface along the ET reaction path

For the theoretical description of the reaction path the transferred charge has to be considered as well. P and S might have a similar atomic configurations, however, the local change in charge is tremendous when the electron is transferred. The already mentioned Franck Condon Principle rules out an equilibrium between the solvent – approximated as dielectric continuum – and the TS. Only the electronic polarization of the solvent molecules can respond fast enough to satisfy the requirement of conservation of energy. With this approximations Marcus derived the analytical expression in equation 1.14 for ΔG^* in order to finally calculate the reaction rate. This expression is valid if at least one reactant is uncharged – otherwise a Coulombic work term has to be added – and if contributions from electron tunnelling are negligible. In most cases the electronic interaction is weak so that V_{PS} can be neglected as well.

$$\Delta G^* = \frac{\lambda}{4} \left(1 + \frac{\Delta G^\circ}{\lambda} \right)^2 - V_{PS} \quad (1.14)$$

The driving force ΔG° is calculated from equation 1.15 where E_A and E_D denote the redox potentials and z_A and z_D the charge of the reactants. Further, F denotes the Faraday constant, e_0 the elementary charge, ϵ_s the dielectric constant of the solvent, f_{DH} the activity coefficient from Debye-Hückel and σ the reaction distance.

$$\Delta G^\circ = -F(E_A - E_D) + (z_A - z_D + 1) \frac{e_0^2 f_{DH}}{\epsilon_s \sigma} \quad (1.15)$$

The quadratic dependence of ΔG^* on ΔG° in equation 1.14 predicts an unusual trend. Per definition the driving force is negative and fast rates are associated with large values of ΔG° . Due to the quadratic dependence, however, this trend is inverted after reaching the maximum at a value of $\Delta G^\circ = -\lambda$. This so called inverted region was an experimental challenge for many decades since the difference in redox potentials is limited. In the mid 1980ies this problem was overcome by studying intramolecular ET in photochemical systems where the absorbed photon energy adds to the net driving force. This solution additionally solves issues from the limit of diffusion which is required to establish close contact in bimolecular systems. [1.13] Unfortunately bimolecular systems tend to converge towards the rate of diffusion upon increasing the driving force which lead to the semi empirical extension by Rehm and Weller in equation 1.16. [1.14] This equation does not postulate the inverted region any more.

$$\Delta G^* = \frac{\Delta G^\circ}{2} + \sqrt{\left(\frac{\lambda}{4}\right)^2 + \left(\frac{\Delta G^\circ}{2}\right)^2} \quad (1.16)$$

The best proof for the original concept of the inverted region, however, was delivered a few years ago. The superior time resolution of femtosecond laser spectroscopy was used to study quenching of excited fluorophores by ET beyond the limits of diffusion. These experiments ultimately proof that the findings of Rehm and Weller were arising from the inferior time resolution of steady state methods. Therefore it is just an experimentally induced artefact instead of a real physical concept and therefore the initial prediction of Marcus is valid nonetheless. [1.15]

1.4 Concept and Study of Reorganization

Figure 1-2 illustrates the process of ET from equation 1.13 in more detail in order to explain the concept of reorganization which is a consequence of the Franck Condon Principle. The blue circles show the reactants in different geometries as indicated by the size and the black and white ellipsoids correspond to polar solvent molecules.

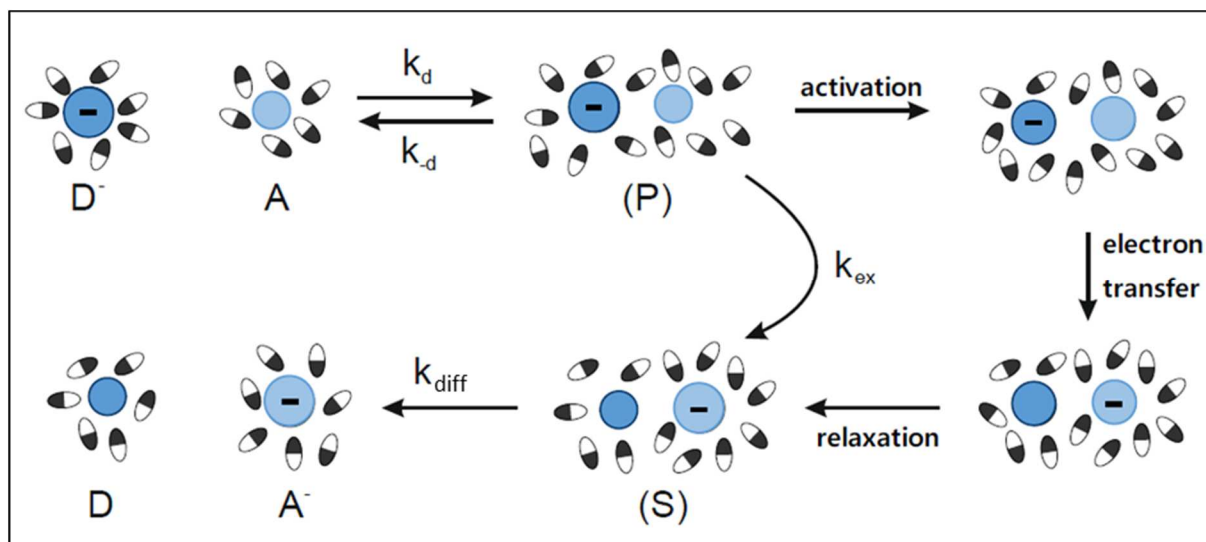


Figure 1-2: Illustration of an ET reaction

In order to stabilize the electron after a transfer the system needs to be in the configuration of the successor which requires changes in the reactants configuration and the solvent orientation. As already mentioned the electron moves faster than all nuclei in the reactants and solvent molecules thus this reorganization needs to occur before the transfer. In figure 1-2 this is indicated by the new additional activation step. The required energy is summarized in the reorganization energy λ which is separated in contributions from the reactants – inner sphere reorganization energy λ_i – and the solvent – outer sphere reorganization energy λ_o that are connected additively.

In order to rearrange the reactants geometry bond lengths and angles need to be changed. The general definition of λ_i is displayed in equation 1.17. Here f_i is the reduced force constant associated with the change of the equilibrium values for the normal mode coordinates Q or reactants r and products p .

$$\lambda_i = \frac{1}{2} \sum_i f_i (Q_i^r - Q_i^p) \quad (1.17)$$

For complex molecules it is rather difficult to identify all vibrational modes that contribute to this reorganization and calculate the corresponding force constants from the first derivative of the potential energy surface. The most abundantly applied solution to this issue is the approximation by the method of Nelsen who showed that mapping four distinct points along the reaction path is sufficient. [1.16] He calculated the absolute energy of these points by quantum chemical methods and used them to estimate according to equation 1.18. The nomenclature here works as follows: $E_{A,A}$ is the energy of the acceptor in its ground state, $E_{A,D}$ the energy of the acceptor in the geometry of the donor and so forth.

$$\lambda_i = (E_{A,D} + E_{D,A}) - (E_{A,A} + E_{D,D}) \quad (1.18)$$

The problem with the initial concept of λ_i is that it is only valid under the high temperature approximation that states all vibrational frequencies $\nu \ll k_B T/h$. At lower temperatures, however, electron tunnelling might be effective and has therefore to be included. Equation 1.19 displays the corresponding correction according to Holstein [1.17] where ν' is the mean vibration frequency of the entire system, k_B the Boltzmann constant and T the absolute temperature.

$$\lambda_i^{\text{corr}} = \lambda_i \frac{4k_B T}{h\nu'} \tanh\left(\frac{h\nu'}{4k_B T}\right) \quad (1.19)$$

As already mentioned in the previous chapter the solvent dipoles have to correspond to the shift of the charge as well as illustrated in figure 1-2. Marcus described this in terms of a position dependent dielectric polarization function which originates in the field of electrostatics. Here a chemically more intuitive approach will be used instead. The overall polarization \vec{P} of a molecule is determined by the sum of two contributions arising from permanent \vec{P}_p and induced dipole moments \vec{P}_i . Since the change of a permanent dipole moment requires to move the entire molecule this is the limiting contribution. The slow contribution to \vec{P}_i is displayed in equation 1.20. Here \vec{D} denotes the electric induction displacement, ϵ_0 the vacuum permittivity and γ the Pekar factor which is defined from the refractive index n and the relative permittivity of the solvent ϵ_s in equation 1.21.

$$\vec{P}_i = \frac{\gamma}{4\pi\epsilon_0} \vec{D} \quad (1.20)$$

$$\gamma = \frac{1}{n^2} - \frac{1}{\epsilon_s} \quad (1.21)$$

Integrating \vec{P}_i over the volume under the assumption that the reactants are spherical yields the energy associated with λ_o as displayed in equation 1.22.

$$\lambda_o = \frac{e_0^2 \gamma}{4\pi\epsilon_0} \left(\frac{1}{2r_A} + \frac{1}{2r_D} - \frac{1}{\sigma} \right) \quad (1.22)$$

In his original theory Marcus did not only separate the reorganization of reactants and solvent but also the reorganization of the two individual reactants. In this case the overall reorganization energy would be the sum of inner and outer reorganization of each reactant individually.

There is no experiment to directly measure single reactant energetics to proof this prediction, however, the study of so-called electron self-exchange is an elegant way to circumvent this

problem. It is an isoenergetic process in between reactants of the same molecule that differ only in the oxidation state as displayed in equation 1.23.



Since $\Delta G^{\circ} = 0$ for this type of process equation 1.14 simplifies to equation 1.24 where V_{PS} is assumed to be negligible small. In this case ΔG^* is dependent on λ only which allows to directly determine the reorganization energy from an experiment.

$$\Delta G^* = \frac{\lambda}{4} \quad (1.24)$$

We further assume the absolute value of the energy required to reorganize A to A^{\bullet} to be equal to the one going from A^{\bullet} to A. Then single reactant reorganization energy is half of the one from the self-exchange.

If now the assumption $\lambda_{AD} = \lambda_A + \lambda_D = \frac{1}{2} (\lambda_{AA} + \lambda_{DD})$ is inserted in equation 1.24 in order to solve the overall rate expression in equation 1.12 the so-called Marcus Cross Relation is obtained. Its common form is displayed in equation 1.25 with k_{AD} being the rate of the cross reaction and k_{AA} and k_{DD} the ones of the self-exchange. The equilibrium constant K is determined from the redox potentials E_A and E_D as displayed in equation 1.26 and the factor f is defined in equation 1.27 where the preexponential factor was approximated as collision frequency Z.

$$k_{AD} = \sqrt{fk_{AA}k_{DD}K} \quad (1.25)$$

$$K = \exp\left(\frac{nF}{RT}(E_A - E_D)\right) \quad (1.26)$$

$$f = \frac{\ln(K)^2}{4 \ln\left(\frac{k_{AA}k_{DD}}{Z^2}\right)} \approx 1 \quad (1.27)$$

Even though these assumptions on the additivity of λ seem to oversimplify the physical issues conclusive experimental evidence on the validity of the Marcus Cross Relation exists. [1.18]

1.5 The Preexponential Factor

So far only the exponential term which is also denoted as nuclear factor κ_n of the rate expression in equation 1.12 was discussed. In equation 1.11 the preexponential factor, however, was already displayed as product of different contributions from statistical mechanics. These are now translated in more experimentally relevant parameters where the product of two terms – the nuclear frequency ν_n and the already mentioned electronic factor κ_{el} – account for the preexponential factor. [1.19]

In the original publication Marcus used a collision model in gas-phase to describe ν_n which is describing the frequency of crossing the activation barrier. The result is displayed in equation 1.28 where σ^2 is the reactive cross section, N_A the Avogadro constant and M the molecular mass.

$$\nu_n = \sigma^2 N_A \sqrt{\frac{16\pi RT}{M}} \quad (1.28)$$

This first description is too simplified since the vibrational modes of the solvent need to be included as well. So the overall nuclear frequency is rewritten as the sum of all contributions of the reactants i and the solvent o . In equation 1.29 they were additionally weighted by their respective reorganization energy.

$$\nu_n = \sqrt{\frac{\nu_i^2 \lambda_i + \nu_o^2 \lambda_o}{\lambda}} \quad (1.29)$$

In the context of the outer sphere reorganization energy in chapter 1.4 the slow polarization must be considered due to the same arguments. In the description of ν_n it was introduced in terms of the longitudinal relaxation time τ_L that is defined by the Debye relaxation time τ_D according to equation 1.30. Here V_M denotes the molar volume, ϵ_s the static dielectric constant of the solvent, ϵ_∞ the infinite frequency dielectric constant and η the dynamic viscosity.

$$\tau_L = \frac{\epsilon_\infty}{\epsilon_s} \tau_D = \frac{\epsilon_\infty}{\epsilon_s} \frac{3V_M \eta}{RT} \quad (1.30)$$

Even though this so-called solvent friction was suggested already in 1940 [1.20] it took a while to formulate a final theory. Several authors [1.21] were included in this process to develop models for several different problems. In equation 1.31 one of the simplest solutions that assumes that $\lambda_i \ll \lambda_o$ is presented.

$$\nu_n = \frac{1}{\tau_L} \sqrt{\frac{\lambda_o}{4\pi RT}} \quad (1.31)$$

The second contribution κ_{el} to the preexponential factor is of a more quantum mechanical origin. As already mentioned in chapter 1.2 it describes the probability of the system leaving the TS. An analytical solution for this probability was derived independently by Landau and Zener in the early 1930ies. [1.22] Equation 1.32 displays the solution in the context of ET in the high temperature limit where ν_n denotes the previously discussed nuclear frequency and ν_{el} an electronic frequency that is given in equation 1.33. It is dependent on the square of V_{PS}

which is usually calculated by quantum chemical methods or estimated from experimental charge transfer bands according to the method of Hush. [1.23]

$$\kappa_{\text{el}} = \left[\frac{2 \left(1 - \exp\left(\frac{-\nu_{\text{el}}}{2\nu_n}\right) \right)}{2 - \exp\left(\frac{-\nu_{\text{el}}}{2\nu_n}\right)} \right] \quad (1.32)$$

$$\nu_{\text{el}} = \frac{2V_{\text{PS}}^2}{h} \sqrt{\frac{\pi^3}{RT(\lambda_i + \lambda_o)}} \quad (1.33)$$

At this point two types of types of ET can be distinguished. If V_{PS} is large so that $\nu_{\text{el}} \gg 2\nu_n$ the reaction is called adiabatic with $\kappa_{\text{el}} = 1$. In this case the reaction crosses the barrier as expected. If, however, V_{PS} is small so that $\nu_{\text{el}} \ll 2\nu_n$ then $\kappa_{\text{el}} = \nu_{\text{el}}/\nu_n$ which eliminates ν_n from the preexponential factor. In this case the reaction is called diabatic and the system has the possibility to reach high-energy states above the TS. These two types of ET can be distinguished experimentally by the method of Weaver [1.24] which will not be explained in detail here due to the insignificant relevance to the experimental work.

1.6 Application to PCET

The idea of expanding the concepts in Marcus theory to other types or transfer processes started relatively early with proton transfer. Relevant concepts for this contest are nicely summarized in a review article by Silverman. [1.25]

For process of PCET, however, this approach is relatively new since this summarizes a whole set of different reaction mechanisms. There are various distinguishable stepwise mechanisms where various sets of orbitals and transferred particles can be involved, a concerted one which is also called hydrogen atom transfer (HAT) and various so-called hybrid-mechanisms. [1.26] This complicates the development of a unified theory significantly, even though just at the end of last year a first general rate expression was published. It attributes for various aspects of PCET but the direct applicability to experiments is still limited. [1.27]

Therefore a simpler alternative approach was developed that uses the same concepts of Marcus theory [1.28] and conclusively proven by experiments. [1.29] The focus of this work was on HAT since it is the least complicated mechanism as well as the predominant reaction path for organic radicals. The most significant differences to ET is that a chemical bond has to be broken and formed. Further, the precursor and successor states have a relatively strong electronic interaction via a hydrogen bond.

First of all the overall rate is expressed in terms of TST as well and developed under the same assumptions of Marcus theory for adiabatic level crossings. The picture in figure 1-1 is only slightly changed since the reaction now starts from the vibrational ground state of the proton which is introduced by considering the related zero point energy E_{ZP} . Therefore the original Marcus equation for the activation barrier – refer to equation 1.14 – is extended for ΔZPE as shown in equation 1.34 where V_{PS} is neglected.

$$\Delta G^* = \frac{\lambda}{4} \left(1 + \frac{\Delta G^\circ}{\lambda} \right)^2 - \frac{\Delta E_{ZP}}{RT} \quad (1.34)$$

Franck Condon Principle is then extended to a single proton as well which still moves faster than all other nuclei so that amongst others the entire concept around the Marcus Cross relation remains valid. The new outer sphere reorganization energy λ_o is divided in two independent contributions for ET and PT even though the transfer is considered to occur in a concerted mode. Equation 1.35 describes the reorganization in respect to the ET and equation 1.36 to the PT for two spherical molecules with $r_A = r_D$ in close contact. The new variable μ denotes the dipole moment of reactants R and products P.

$$\lambda_o^{ET} = \frac{e_0^2 \gamma}{4\pi\epsilon_0} \left(\frac{1}{2r_A} \right) \quad (1.35)$$

$$\lambda_o^{PT} = \frac{1}{4\pi\epsilon_0} \left[\left(\frac{\epsilon_s - 1}{2\epsilon_s + 1} \right) \left(\frac{n^2 - 1}{2n^2 + 1} \right) \right] \left(\frac{(\mu_R - \mu_P)^2}{r_A^3} \right) \quad (1.36)$$

Finally the preexponential factor is developed as product of a collision frequency and an electronic factor as well. The latter is again developed in the Landau-Zener framework and yields a dependence on the square of V_{PS} .

Large kinetic isotope effects for the transfer of hydrogen and deuterium, however, showed that proton tunnelling contributions impact HAT kinetics rather extensively. [1.30] Therefore alternative descriptions for this electronic coupling are currently developed from quantum mechanical considerations which are up to now not easily applicable to experiments.

1.7 References

- [1.1] H. Chan, T.N. Cong, W. Yang, C. Tan, Y. Li and Y. Ding, *Prog. Nat. Sci.* 19, 291 (2009)
- [1.2] L. El Chaar, L.A. Lamont and N. El Zein, *Renew. Sustainable Energy Rev.* 15, 2165 (2011)
- [1.3] a) B.A. Diner, D.A. Force, D.W. Randall and R.D. Britt. *Biochemistry* 37, 17931 (1998)
b) K. Möbius, A. Savitsky and M. Fuchs. *Biolog. Magn. Res.* 22, 45 (2004)
- [1.4] a) M. Sjödin, S. Styring, B. Åkermark, L. Sun and L. Hammarström, *J. Am. Chem. Soc.* 122, 3932 (2000)
b) F. Ogliaro, S. Cohen, M. Filatov, N. Harris and S. Shaik, *Nature* 40, 647 (2001)
- [1.5] H. Pellissier, *Tetrahedron* 63, 9267 (2007)
- [1.6] a) R.A. Marcus, *J. Chem. Phys.* 24, 966 (1956)
b) R.A. Marcus, *J. Chem. Phys.* 26, 867 (1957)
c) R.A. Marcus, *J. Chem. Phys.* 26, 872 (1957)
- [1.7] R.A. Marcus, *Rev. Mod. Phys.* 65, 599 (1993)
- [1.8] a) R.D. Cannon, *Electron Transfer Reactions*, Butterworth (1980)
b) A.M. Kuznetsov and J. Ulstrup, *Electron Transfer in Chemistry and Biology: An Introduction to the Theory*, Wiley (1999)
c) V. May and O. Kühn, *Charge and Energy Transfer Dynamics in Molecular Systems*, Wiley VCH (2011)
- [1.9] a) N. Sutin, *Ann. Rev. Nucl. Sci.* 12, 285 (1962)
b) N. Sutin, *Progr. Inorg. Chem.* 30, 441 (1983)
c) S.J. Formosinho, L.G. Arnaut and R. Fausto, *Prog. React. Kinet.* 23, 11 (1998)
- [1.10] a) C. Constantin, *Chem. Rev.* 108, 2145 (2008)
b) J.J. Warren and J.M. Mayer, *Proc. Natl. Acad. Sci.* 107, 5282 (2010)
c) J.M. Mayer, *J. Phys. Chem. Lett.* 2, 1481 (2011)
- [1.11] H. Eyring, *J. Chem Phys.* 3, 115 (1935)
- [1.12] G.M. Barrow, *Physical Chemistry Sixth Edition*, McGraw-Hill Inc. (1996)
- [1.13] a) J.R. Miller, L.T. Calcaterra and G.L. Closs, *J. Am. Chem. Soc.* 106, 3047 (1984)
b) G.L. Closs, L.T. Calcaterra, N.J. Green, K.W. Penfield and J.R. Miller, *J Phys. Chem.* 90, 3673 (1986)
- [1.14] D. Rehm and A. Weller, *Berichte der Bunsen-Gesellschaft* 73, 834 (1969)
- [1.15] A. Rosspeintner, A. Gonzalo and E. Vauthey, *J. Am. Chem. Soc.* 136, 2026 (2014)
- [1.16] F.S. Nelsen, S.C. Blackstock and Y. Kim, *J. Am. Chem. Soc.* 109, 677 (1987)

- [1.17] T. Holstein, *Phil. Mag. Part B* 37, 49 (1978)
- [1.18] a) R.A. Marcus and N. Sutin, *Biochimica et Biophysica Acta* 811, 265 (1985)
b) G. Grampp, S. Landgraf, D. Sabou and D. Dvoranova, *J. Chem. Soc. Perkin Trans. 2*; 178 (2002)
- [1.19] N. Sutin, *Acc. Chem. Res.* 15, 275 (1982)
- [1.20] H. Kramers, *Physica (The Hague)* 7, 284 (1940)
- [1.21] a) H. Sumi and R.A. Marcus, *J. Chem. Phys.* 84, 4894 (1986)
b) I. Rips and J. Jortner, *J. Chem. Phys.* 87, 2090 (1987)
c) I. Rips and J. Jortner, *J. Chem. Phys.* 87, 6513 (1987)
d) L.D. Zusman, *Chem. Phys.* 119, 51 (1988)
e) M. Bixon and J. Jortner, *Chem. Phys.* 176, 467 (1993)
- [1.22] a) L. Landau, *Phys. Zeitschr. d. Sov. Union* 2, 46 (1932)
b) C. Zener, *Proc. Royal Soc. London A* 137, 696 (1932)
- [1.23] a) N.S. Hush, *Trans. Faraday Soc.* 57, 557 (1961)
b) N.S. Hush, *Eletrochim. Acta* 13, 1005 (1968)
- [1.24] a) M.J. Weaver and G.E.I. McManis, *Acc. Chem. Res.* 23, 294 (1990)
b) M.J. Weaver, *Chem. Rev.* 92, 463 (1992)
- [1.25] D.N. Silverman, *Biochimica et Biophysica Acta* 1458, 88 (2000)
- [1.26] M.H.V. Huynh and T.J. Meyer, *Chem. Rev.* 107, 5004 (2007)
- [1.27] S. Hammes-Schiffer and A.V. Soudackov, *Faraday Discuss.* 195, 171 (2016)
- [1.28] C. Constantini, *Chem. Rev.* 108, 2145 (2008)
- [1.29] J.M. Mayer, *J. Phys. Chem. Lett.* 2, 1481 (2011)
- [1.30] A. Wu, E.A. Mader, A. Datta, D.A. Hrovat, W.T. Broden and J.M. Mayer, *J. Am. Chem. Soc.* 131, 11985 (2009)

2. ESR Spectroscopy

2.1 Introduction

Electron Spin Resonance spectroscopy (ESR) is in principle an absorption technique that is also known as Electron Paramagnetic Resonance spectroscopy (EPR) or Electron Magnetic Resonance (EMR) spectroscopy. It is closely related to Nuclear Magnetic Resonance spectroscopy (NMR) which is more commonly applied in the field of chemistry.

Both methods utilize the magnetic Zeeman Effect which was already observed experimentally in 1896. [2.1] It took about three decades to interpret this results nevertheless. Similar experiments in the early 1920ies [2.2] led to the formulation of the spin itself as intrinsic quantum mechanical property of matter. The interaction of electronic magnetic moments induced by unpaired spins and a magnetic field create non degenerate energy levels. By an oscillating field of an electromagnetic wave direct transitions are allowed; thus resulting in absorption. The energy of the ESR transitions is in the microwave region.

From a technological point of view all magnetic resonance methods originated around the end of World War II since it caused a tremendous progress in the field of radar technology. The first successful ESR experiment was reported in the Soviet Union in 1945. [2.3] Approximately one year later the same was achieved independently in the United States. [2.4] Right about the same time the first NMR experiments were performed by various groups. [2.5]

The limitation to paramagnetic systems – these contain unpaired electron spins by definition – is the reason that the method is significantly less prevalent in the field of chemistry. These systems include free radicals with one or more radical centres, triplet state molecules, transition metal ions and defects in crystals where except for the last example any state of aggregation is accessible. Especially in complex biological systems, chemical catalysis, semiconductors etc. paramagnetic systems play a major role. ESR can provide insight in the valence states, binding situations and structure of a molecule or complex, the surrounding of a molecule or complex (e.g. type of hydration or distance between paramagnetic centres) and its dynamics such as diffusion, rotation and exchange and sometimes even in the quantity of the paramagnetic species. For this last analytical application the limitation is a major advantage in terms of sensitivity since in general most of the general matrix is not paramagnetic.

A large number of textbooks is available on the theory of ESR spectroscopy which differ strongly in the degree of insight and clarity dependent on the application emphasized by the author. For a general introduction to the field the textbook of Gerson and Huber [2.6] and an online accessible script of the University of Konstanz by G. Jeschke [2.7] are recommendable. In this work the focus is explicitly on the study of kinetics of chemically relevant dynamics in solution which will be presented in the following chapters. This is nicely addressed in the books of Weil - Bolton [2.8] and Scheffler - Stegmann. [2.9] More recent developments will be cited directly from scientific literature in the relevant chapters.

2.2 Fundamentals of Magnetic Resonance

In order to observe magnetic resonance the partitioning energy levels need to be generated by a magnetic field so-to-speak. In ESR spectroscopy these energy levels are associated with the electron's spin S which has values of $\pm \frac{1}{2}$. The spin is an intrinsic quantum mechanical property that mathematically behaves like an orbital angular momentum that is expressed by an angular momentum vector \vec{S} . It's general expression is given in equation 2.1 where h denotes the Planck constant.

$$|\vec{S}| = \frac{h}{2\pi} \sqrt{S(S+1)} \quad (2.1)$$

Since the electron is a charged particle a magnetic moment $\vec{\mu}_e$ can be assigned to this quasi motion. Equation 2.2 shows different ways to express this magnetic moment. g_e denotes the dimensionless g-factor, e_0 the elementary charge, m_e the mass of the electron, μ_B the Bohr magneton and γ_e the gyromagnetic ratio.

$$\vec{\mu}_e = -\frac{g_e e_0 \vec{S}}{2m_e} = -\frac{2\pi g_e \mu_B \vec{S}}{h} = \gamma_e \vec{S} \quad (2.2)$$

For unpaired electrons this free magnetic moment is able to interact with an external magnetic field. In the following the magnetic field \vec{H} will be expressed as magnetic flux density \vec{B} which is the standard in ESR literature. Note that \vec{B} is simply the product of \vec{H} and the magnetic permeability μ_m . The direction of this field is set to the z-axis throughout the whole text.

This interaction has two important consequences for the free electron spins which are illustrated in figure 2-1. Note that magnetic field lines point from are defined to point from the north to the south pole, whereas magnetic moments are defined in the opposite direction.

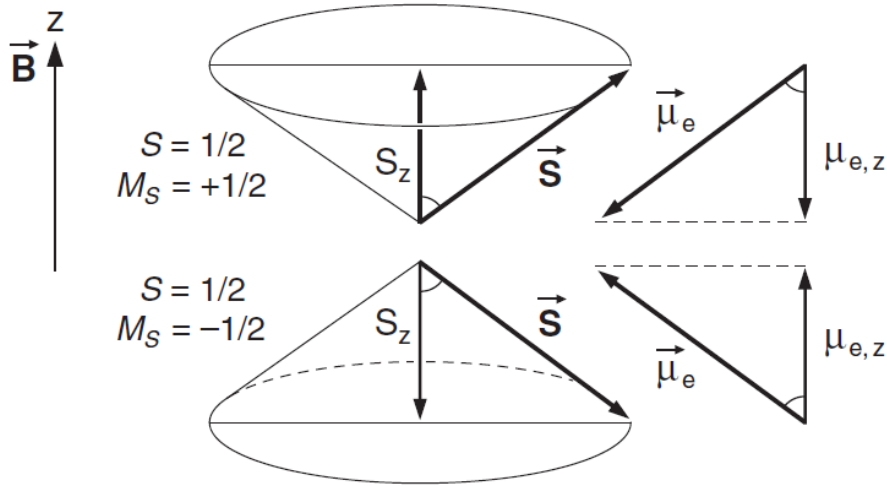


Figure 2-1: Schematic display of a free electron spin in an external magnetic field [3.6.]

The first consequence of the interaction is that the spins start to rotate around the field lines in a precession mode on a stable orbit with the so called Larmor frequency ω_B in equation 3.3.

$$\omega_B = \gamma_e B_z \quad (2.3)$$

The second is that the new non-degenerate energy states – the so-called Zeeman Effect – arise due to the fact that the spin is a quantized property. The effective Hamiltonian \hat{H} is displayed in equation 3.4 in dependence of the effective Spin operator in the z-direction \hat{S}_z .

$$\hat{H} = -\hat{\mu} * \hat{B} = g_e \mu_B B_z \hat{S}_z \quad (2.4)$$

The eigenvalues to this Hamiltonian provide the energy E of an oriented spin according to equation 2.5 as function of the spin quantum number m_s which is the z-projection of the vector \vec{S} . There are $2S+1$ values for m_s with the absolute values of $\{S, S-1, \dots -S\}$. To each quantum number m_s one so-called spin state exists.

$$E = m_s g_e \mu_B B \quad (2.5)$$

Due to the fact that the spin S of an electron is $\frac{1}{2}$ there are only two orientations possible that correspond to $m_s \pm \frac{1}{2}$. The more stable spin state – meaning $m_s = -\frac{1}{2}$ – is usually called α -spin, the other one β -spin. Subtracting the energy of α - and β -spin yields the equation 2.6

$$\Delta E = g_e \mu_B B \quad (2.6)$$

The relative populations of the two spin states in thermal equilibrium with their surroundings are generally expressed by the Boltzmann distribution in equation 2.7. There n denotes the number of spins in the specific state, k_B the Boltzmann constant and T the given temperature.

$$\frac{n_\beta}{n_\alpha} = \exp\left(\frac{\Delta E}{k_B T}\right) \quad (2.7)$$

If the energy of an electromagnetic wave matches the energy difference of these spin states transitions with $\Delta m_s = \pm 1$ are allowed. This energy is universally defined as product of the Planck constant h and the frequency ν of the radiation. Using the law of conservation of energy this can be inserted in equation 2.6 which yields the resonance condition 2.8.

$$\nu = \frac{g_e * \mu_B * B}{h} \quad (2.8)$$

2.3 Technological Considerations

For a general introduction into the functionality of the components and devices the book of Ishii is highly recommended as well as the more advanced of Poole. [2.10] This chapter only deals with two special aspects that are required to understand the spectra presented in the experimental section.

Firstly the energy on the x-axis of all spectra will be presented in units of the magnetic field strength. This is related to the fact that in contrast to most other spectroscopic methods the frequency of the radiation is kept constant while the magnetic field is swept. Therefore one can often find the abbreviation CW-ESR

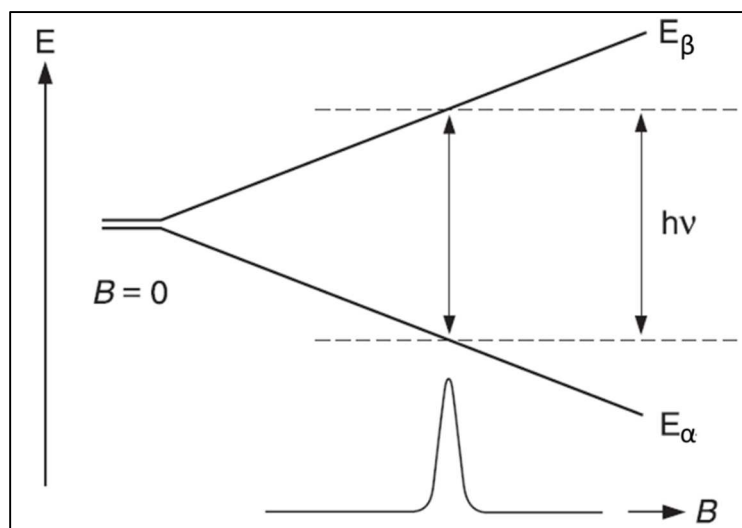


Figure 2-2: Schematic operation of an ESR experiment [3.6]

which stands for continuous wave ESR. Figure 2-2 displays this operating mode schematically where an absorption spectrum is drawn at the position of the possible transition.

The second particularity is that all spectra are presented as the first derivative of the absorption signal since they are recorded in this way. In order to improve the signal to noise ratio an additional oscillating magnetic field B_m is generated in the cavity by the so-called modulation coils. The frequency of this oscillation is superimposed to the recorded signal as displayed in figure 2-3 at one specific value of B . The detector then records the difference of the maximum amplitudes which corresponds to the slope at this point thus resulting in the first derivative display. Upon implementing frequency selective detection most of the noise can be eliminated which improves the signal tremendously.

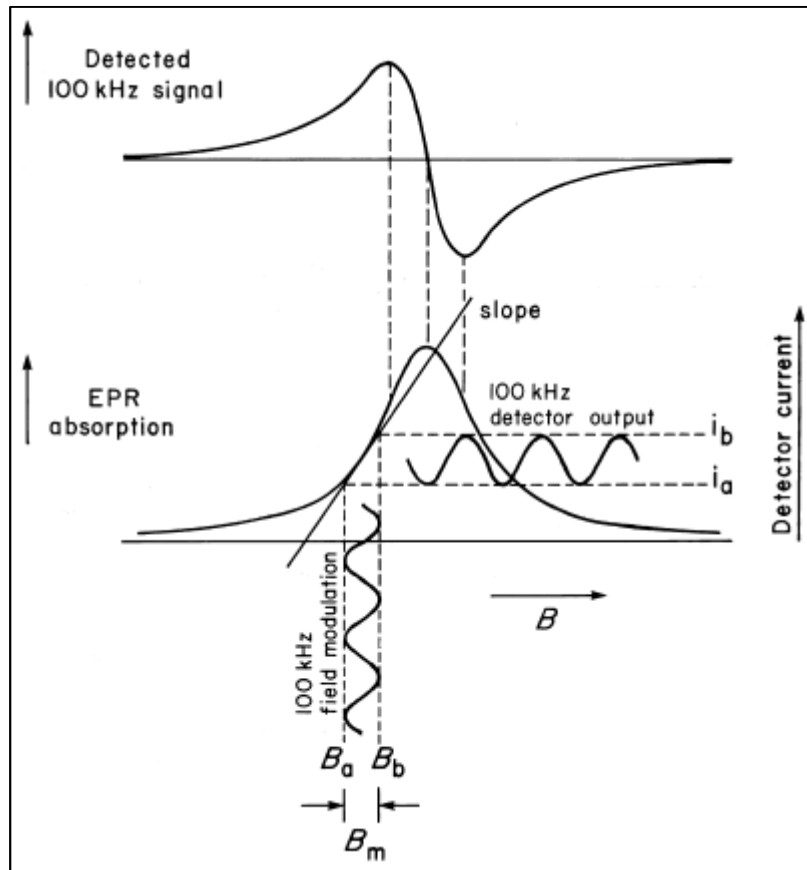


Figure 2-3: Schematic operation of the modulation [3.6]

Besides the advantage for the signal to noise ratio, however, the modulation also causes the operator to a certain compromise between spectral resolution and signal intensity. If the spectrum has multiple lines a large modulation amplitude will blur them into less and broader lines. The signal intensity on the other side is proportional to the modulation amplitude squared since the detector records the difference at maximum amplitude. This fact leads to the circumstance that some spectra cannot be resolved since over modulating them is required to obtain a signal at all.

2.4 The static ESR Spectrum

In general the spectrum is a simple plot of the recorded signal intensity in arbitrary units versus the energy of the transition in units of a magnetic field strength. (see chapter 2.2) Usually the spectral lines correspond to the first derivative of a Lorentzian function (2.9) which is the case for this work. However, there are a few metal complexes where the first derivative of a Gaussian (2.10) is observed instead. A stands for absorption, Γ denotes the half width at half maximum (HWHM) – in the experimental section the peak-to-peak line-width ΔB_{PP} used instead – and B_r the central field of the actual transition.

$$A' = -A_{max} \frac{2 * \Gamma^2 * (B - B_r)}{(\Gamma^2 + (B - B_r)^2)} \quad (2.9)$$

$$A' = -A_{max} \left[\frac{2 * \ln(2) * (B - B_r)^2}{\Gamma^2} \right] \exp \left[- \frac{\ln(2) * (B - B_r)^2}{\Gamma^2} \right] \quad (2.10)$$

Figure 2-4 displays an experimental ESR spectrum of our calibration standard the perylene radical cation. It will be used to explain the informational content of a spectrum.

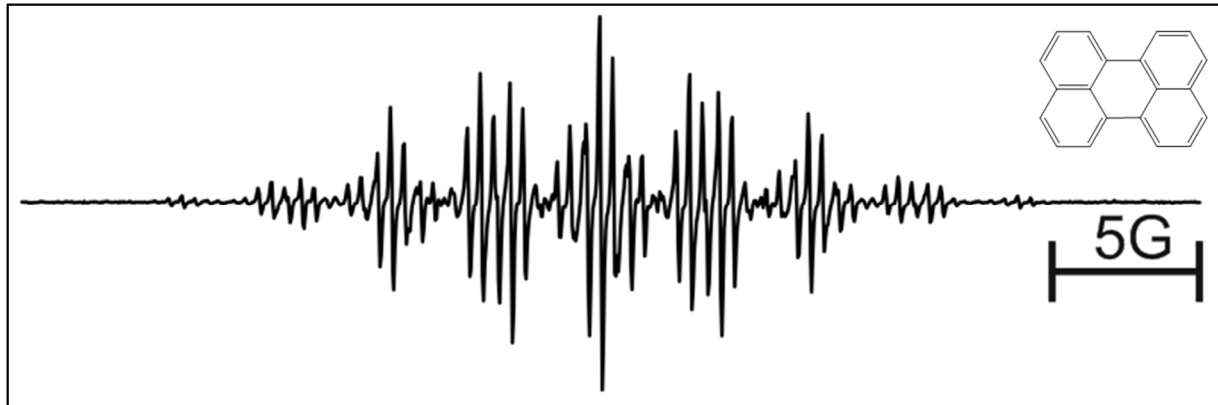


Figure 2-4: Structure of perylene and experimental spectrum of the corresponding radical cation

First of all the spectrum contains qualitative information. From the centre of the spectrum the g-factor could be calculated at the given frequency from equation 2.8. Similar to the chemical shift in NMR spectroscopy it is defined by the chemical environment of the spin and therefore specific to the system. However, the changes in g-factors are significantly smaller. For organic radicals they start to differ at position five or more after the decimal point which is a serious challenge for experimentalists.

If the spectrum is integrated twice one obtains an area that is a measure for the signal intensity. The overall absorbed microwave power P_A is given in equation 2.11. The variables B_1 , τ_1 and τ_2 will be explained in chapter 2.5. Further equation 2.12 defines the static magnetic susceptibility χ^0 which is dependent on the number of free spins per Volume N_V and a dimensionless factor κ which accounts for the surrounding medium.

$$P_A = \frac{\omega B_1^2}{\mu_0} \frac{\pi \chi^0 B_r}{(1 + \gamma_e^2 B_1^2 \tau_1 \tau_2)} A(\omega - \omega_B) \quad (2.11)$$

$$\chi^0 = \frac{\kappa g^2 \mu_B^2 \mu_0}{4k_B} * \frac{N_V}{T} \sim \frac{C}{T} \quad (2.12)$$

The dependence on N_V makes the area a measure for the radical concentration equivalent to NMR spectroscopy. In the context of quantitative analytics the limitation to paramagnetic species is a major advantage. However, there is a strong temperature dependence of the static magnetic susceptibility – thermal motion disturbs the orientation of the spins – and the

problem that the noise is integrated twice as well. This problems and adequate solutions are comprehensively discussed in a rather recent textbook. [2.11]

The most visible feature of the spectrum displayed in figure 2-4 is the multitude of lines which is related to the so-called hyperfine splitting. It originates from the interaction of the electron spin with spins I of magnetically active nuclei. These nuclear spins which are not restricted to values of $\pm \frac{1}{2}$ interact in the same way as the free electron spin. Therefore the energy of the resulting nuclear spin states is obtained by the analogue Hamiltonian in equation 2.13 with the corresponding nuclear g-factor g_n , a nuclear magneton μ_n and an effective Spin operator in the z-direction \hat{I}_z .

$$\hat{H} = -\hat{\mu} * \hat{B} = g_n \mu_n B_z \hat{I}_z \quad (2.13)$$

There are two types of interactions between the different spins. One is the anisotropic dipole-dipole interaction, the other the isotropic so-called Fermi contact interaction. The classical dipole-dipole interaction requires the spins to be strongly aligned in the field. Meeting this requirement the resulting energy E_{dip} is calculated according to equation 2.14. Figure 2-5 illustrates how the distance r and the angle θ are defined relative to the external field B . Further μ_0 denotes the vacuum permeability.

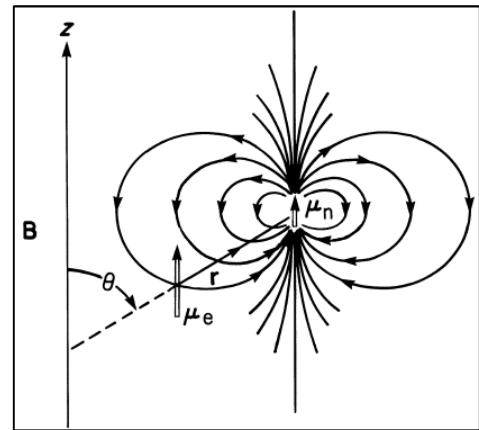


Figure 2-5: Illustration of the dipole-dipole interaction

$$E_{dip} = \frac{\mu_0 * \mu_B * \mu_N}{4\pi * r^3} * (3 \cos^2 \theta - 1) \quad (2.14)$$

The molecules are highly mobile in solution thus the effective average of the dipole-dipole interaction over all orientations is usually zero.

In contrast to this the Fermi contact interaction is of purely quantum mechanical origin without any classical analogue. It is an isotropic interaction and therefore also observable in liquid samples. It can be calculated via the Hamiltonian \hat{H}_{FC} in equation 2.15. It requires the calculation of the probability density of finding the electron at the centre of the nucleus $|\Psi_0|^2$. Summarizing all the factors multiplying to the operators' one yields A_0 , which is referred to an isotropic hyperfine coupling constant in energy units (Joule). Conversion from units of Gauss [G] into frequency [MHz] involves the g-value: $A_i[\text{MHz}] = 2.8025(g/g_e)a_i[\text{G}]$.

$$\hat{H}_{FC} = \frac{2}{3} \mu_0 g_e \mu_e g_n \mu_n |\Psi_0|^2 \hat{S}_z \hat{I}_z = A_0 \hat{S}_z \hat{I}_z \quad (2.15)$$

Since $|\Psi_0|^2$ is zero for non s-type orbitals and isotropic hyperfine splitting is observed from α -protons in π -radicals e.g. nonetheless, $|\Psi_0|^2$ was substituted for the spin density at the nucleus $\rho_s(0)$. This description allows further to explain that a_i is experimentally found with either positive or negative sign which can be explained by spin polarization.

Summing up all discussed interactions the effective Hamiltonian \widehat{H}_{eff} for an ESR-sample in solution easily derived from equations 2.4, 2.13 and 2.15. It is displayed in equation 2.16.

$$\widehat{H}_{eff} = g_e \mu_B B_z \widehat{S}_z - \sum g_n \mu_n B_z \widehat{I}_z + \sum A_0 \widehat{S}_z \widehat{I}_z \quad (2.16)$$

For an organic radical with one unpaired spin the amount of Eigenvalues N that correspond to the energy of different non degenerate spin states is derived from equation 2.17. Her n_i denotes the number of equivalent nuclei of the spin I_i .

$$N = 2 * \prod_i^k (2n_i * I_i + 1) \quad (2.17)$$

This means that N/2 transitions are theoretically observable in the spectrum. Going back to the example in figure 2-4 one can readily understand the multitude of lines. Perylene has 3 sets of 4 magnetically equivalent hydrogen atoms with $I = \frac{1}{2}$. Inserting this in equation 2.17 one ends up with individual 125 lines.

The difference in intensity in between two individual lines is related to degenerate transitions and spectral overlap. For simple spectra they can be estimated by simple statistical considerations. If one is looking at nuclei with $I = \frac{1}{2}$ one can simply use Pascal's triangle e.g. where the number of magnetically equivalent nuclei determines the line. For other values of I equivalent aid is provided in every textbook.

2.5 Dynamic ESR

In general the dynamic information is contained in the changes of the spectral line-width. Even though a spectral line corresponds to a transition from one defined energy level to another it is naturally broad due to several reasons. The responsible mechanisms can be distinguished in those that broaden homogeneously and those that broaden inhomogeneously. [2.12]

The inhomogeneous broadening is related to spatial variations in the local magnetic field at different paramagnetic centres which is, however, still constant at one centre itself. In the course of this thesis it was observed once due to molecular rotations in the project discussed in chapter 8.

Homogeneous broadening is related to different mechanisms. On one hand there is the dynamic variation of the local magnetic field at a paramagnetic centre. This fluctuations in time are related to the modulation discussed in chapter 2.3 and molecular motions such as

diffusion. On the other hand there is the so-called lifetime broadening which was of main interest throughout the experimental studies since it is amongst others related to all chemical dynamics such as the exchange of electrons, protons, counter ions, ligands and so forth.

Moreover, there is the alternating line width effect that is related to intramolecular dynamics such as isomerization, ring inversion, proton exchange or restricted rotations. Basically it means that different sets of lines with the same width different from the other set are observed within one spectrum. This will be discussed in the final section of this chapter.

The lifetime broadening originates in the Heisenberg uncertainty principle of energy E and time t which is expressed in terms of ESR spectroscopy in equation 2.18. Note that the uncertainty ΔB is a simple interpretation of a line-width.

$$\gamma_e \Delta B * \Delta t \geq \frac{h}{2\pi} \quad (2.18)$$

The uncertainty in time is related to the lifetime of an excited spin state τ_{ss} which is generated by the observed absorption. Since lifetimes are not commonly used throughout the field of chemistry equation 2.19 translates it into rate constants k . These correspond to all relaxation processes which by definition transfer an individual spin from its excited to the corresponding ground state.

$$\frac{1}{\tau_{ss}} = \sum_{i=1}^n \frac{1}{\tau_i} = \sum_{i=1}^n k_i \quad (2.19)$$

In order to discuss relaxation processes it is easier to look at the system as a whole instead of individual spins. Therefore the magnetization \vec{M} is introduced by equation 2.20 as a macroscopic quantity by simply summing up all magnetic moments. In order to make \vec{M} comparable in-between different systems it is normalized to the volume V .

$$\vec{M} = \frac{1}{V} * \sum_{i=1}^n \vec{\mu}_e \quad (2.20)$$

The change of \vec{M} over time is usually discussed in terms of the operator based Bloch Model which works well for diluted systems and has been applied to fit all experimental data in the course of this work. The alternative matrix based model by Redfield [2.13] will not be discussed here. As displayed in equation 2.21 Bloch simply translates the relaxation to a classical change of angular momentum. Note that \times stands explicitly for the vector product. It, however, neglects effects from the magnetization of emitted photons and/or the attenuation of radiation by the medium.

$$\frac{d\vec{M}}{dt} = \gamma_e * \vec{M} \times \vec{B} \quad (2.21)$$

There are two major physical relaxation processes to consider. One is the so called Spin-Lattice relaxation that simply transfers the excess energy to the surroundings of the excited spin. Therefore it is strongly dependent on temperature. It is associated with the longitudinal relaxation time τ_1 and influences mainly the z-component of \vec{M} .

The other is the so-called Spin-Spin relaxation that describes the loss of phase coherency due to variations in the Larmor frequency. It is associated with the transversal relaxation time τ_2 and influences mainly the x- and y-component of \vec{M} . Equations 2.22-2.24 consider them in a set of coupled differential equations that correspond to equation 2.21. Note that the assumption that τ_2 is independent of τ_1 is mostly justified by the fact that it is usually significantly faster.

$$\frac{dM_x}{dt} = \gamma_e * B * M_y - \frac{M_x}{\tau_2} \quad (2.22)$$

$$\frac{dM_y}{dt} = -\gamma_e * B * M_x - \frac{M_y}{\tau_2} \quad (2.23)$$

$$\frac{dM_z}{dt} = \frac{M_z^0 - M_z}{\tau_1} \quad (2.24)$$

Since relaxation only occurs after excitation by the micro wave its corresponding field \vec{B}_1 needs to be considered. Adding it to equation 2.21 under the consideration of relaxation one obtains a new equation of motion in 2.25. The vectors \vec{i} , \vec{j} and \vec{k} are just unit vectors along the x-, y- and z-axis.

$$\frac{d\vec{M}}{dt} = \gamma_e * \vec{M} \times (\vec{B} + \vec{B}_1) - \frac{\vec{i} M_x + \vec{j} M_y}{\tau_2} - \frac{\vec{k} (M_z^0 + M_z)}{\tau_1} \quad (2.25)$$

Initially Bloch assumed \vec{B}_1 to be circularly polarized. The corresponding components are given in equation 2.26 where ω is the frequency that \vec{B}_1 rotates with.

$$B_{1,x} = B_1 \cos(\omega t); B_{1,y} = B_1 \sin(\omega t); B_{1,z} = 0 \quad (2.26)$$

At this point it has to be considered that usually a linear polarized radiation is used in the experiments. The components of the corresponding oscillating field are given in equation 2.27.

$$B_{1,x} = 2B_1 \cos(\omega t); B_{1,y} = 0; B_{1,z} = 0 \quad (2.27)$$

It can be described as a superposition of two counter-rotating components as given in equation 2.28.

$$2B_1 \vec{i} \cos(\omega t) = B_1 (\vec{i} \cos(\omega t) + \vec{j} \sin(\omega t)) + B_1 (\vec{i} \cos(\omega t) - \vec{j} \sin(\omega t)) \quad (2.28)$$

Since the component in equation 2.28 which is rotating in phase with the Larmor precession is in resonance and hence inducing transitions the other one can be neglected. It is known to induce the so-called Bloch-Siegert shifts which are negligible small.

Separating equation 2.25 in its components upon substituting for equation 2.26 one yields the full description of motion in equations 2.29 – 2.31. These are the so-called Bloch equations.

$$\frac{dM_x}{dt} = \gamma_e * [B * M_y - B_1 * \sin(\omega t) * M_z] - \frac{M_x}{\tau_2} \quad (2.29)$$

$$\frac{dM_y}{dt} = -\gamma_e * [B * M_x - B_1 * \cos(\omega t) * M_z] - \frac{M_y}{\tau_2} \quad (2.30)$$

$$\frac{dM_z}{dt} = \gamma_e * [B_1 * \sin(\omega t) * M_x - B_1 * \cos(\omega t) * M_y] - \frac{M_z^0 - M_z}{\tau_1} \quad (2.31)$$

The Bloch equations were originally solved after transforming the problem in a coordinate system that rotates with the frequency ω around the z-axis. In this coordinate system \vec{B}_1 appears to be stationary and is set to the new x-axis. The transverse magnetization is now expressed by the in phase component u and the 90° off phase component v along the new x- and y-axis in equations 2.32 and 2.33. Figure 2-6 visualizes this new coordinate system.

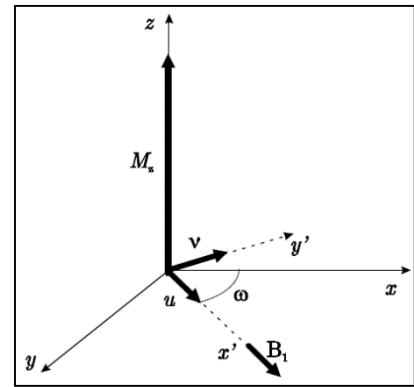


Figure 2-6: Visualization of the rotating coordinate system

$$u = \cos(\omega t) * M_x + \sin(\omega t) * M_y \quad (2.32)$$

$$v = \cos(\omega t) * M_y - \sin(\omega t) * M_x \quad (2.33)$$

For a stationary observer the total change of \vec{M} is now dependent on ω which requires to add an additional term to equation 2.21 as displayed in equation 2.34.

$$\frac{d\vec{M}}{dt} = \gamma_e \vec{M} \times \vec{B} - \vec{M} \times \vec{\omega} = \gamma_e \vec{M} \times \left(\vec{B} + \frac{\vec{\omega}}{\gamma_e} \right) \quad (2.34)$$

The substitution of equation 2.32 in equation 2.25 gives a final set of the Bloch equations in the rotating frame in equations 2.35 – 2.37.

$$\frac{du}{dt} = \gamma_e B v + v \omega - \frac{u}{\tau_2} \quad (2.35)$$

$$\frac{dv}{dt} = -B u - u \omega + \gamma_e M_z B_1 - \frac{v}{\tau_2} \quad (2.36)$$

$$\frac{dM_z}{dt} = -\gamma_e B_1 v - \frac{M_z^0 - M_z}{\tau_1} \quad (2.37)$$

In order to solve this set of coupled differential equations one usually uses a steady state approximation. The solutions are given in equations 2.38 – 2.40. This approximation describes the system after a prolonged continuous irradiation which corresponds nicely to the conditions in a CW-ESR experiment.

$$u = -M_z^0 \frac{\gamma_e B_1 (\omega_B - \omega) \tau_2^2}{1 + (\omega_B - \omega)^2 \tau_2^2 + \gamma_e^2 B_1^2 \tau_1 \tau_2} \quad (2.38)$$

$$v = M_z^0 \frac{\gamma_e B_1 \tau_2}{1 + (\omega_B - \omega)^2 \tau_2^2 + \gamma_e^2 B_1^2 \tau_1 \tau_2} \quad (2.39)$$

$$M_z = M_z^0 \frac{1 + (\omega_B - \omega)^2 \tau_2^2}{1 + (\omega_B - \omega)^2 \tau_2^2 + \gamma_e^2 B_1^2 \tau_1 \tau_2} \quad (2.40)$$

The only τ_1 dependent term $\gamma_e^2 B_1^2 \tau_1 \tau_2$ is the so-called saturation parameter which balances the ratio of relaxation and induced transitions. If B_1 increases the magnetization starts to vanish until total saturation occurs. However, if B_1 goes to zero then u and v go to zero as well whereas M_z approaches its initial value.

So far the ESR experiment has been described without any chemical exchange. In order to handle the following derivations in a more compact way equations 2.35 and 2.36 are combined to the complex magnetization G which is displayed in equation 2.41.

$$\frac{dG}{dt} = \frac{du}{dt} + i \frac{dv}{dt} \quad (2.41)$$

The chemical exchange occurs between two distinguishable states A and B that are interchanged by first order kinetics with the rate constants k_A and k_B as given in equation 2.42. In the further text the exchange process will consistently and exclusively be addressed in terms of rate constants k .



Each rate constant is associated with a lifetime τ according to equation 2.19 which is further associated with the populations p_A and p_B under detailed balance conditions in equation 2.42. The sum of p_A and p_B is always one.

$$\frac{k_B}{k_A} = \frac{\tau_A}{\tau_B} = \frac{p_A}{p_B} \quad (2.43)$$

As long as there is no exchange happening both states have a corresponding complex magnetization G_A and G_B in the form of equation 2.41. Their change can be expressed in terms of chemical rate expressions as in equations 2.44 and 2.45. The new relaxation times T_{2A} and T_{2B} can be understood as inverse line widths of systems without exchange or power saturation.

$$\frac{dG_A}{dt} + G_A \left(\frac{1}{T_{2A}} - i(\omega_{B(A)} - \omega) \right) = \frac{dG_A}{dt} + \alpha_A G_A = -k_A G_A + k_B G_B + i\gamma_A M_{zA} B_1 \quad (2.44)$$

$$\frac{dG_B}{dt} + G_B \left(\frac{1}{T_{2B}} - i(\omega_{B(B)} - \omega) \right) = \frac{dG_B}{dt} + \alpha_B G_B = k_A G_A - k_B G_B + i\gamma_B M_{zB} B_1 \quad (2.45)$$

Assuming steady state conditions these equations can be easily solved to give a total value for the complex transverse magnetization. Note that u and v can still be separated since the latter is in the imaginary part. The solution is given in equation 2.46.

$$G = G_A + G_B = iB_1 M_z \frac{p_A \gamma_A (\alpha_B + k_A + k_B) + p_B \gamma_B (\alpha_A + k_A + k_B)}{(\alpha_A + k_A)(\alpha_B + k_B) - k_A k_B} \quad (2.46)$$

Considering the relation in equation 2.43 G can be alternatively expressed in terms of lifetimes as displayed in equation 2.47.

$$G = iB_1 M_z \frac{\tau_A \tau_B (p_A \alpha_A + p_B \alpha_B) + \tau_A + \tau_B}{(1 + \tau_A \alpha_A)(1 + \tau_B \alpha_B) - 1} \quad (2.47)$$

Since equation 2.47 is due to its complexity not providing a very concrete physical insight a few limiting cases will be considered in order to simplify it. The simplest case assumes very slow exchange where k_A and k_B are considerably smaller than $|\omega_{B(A)} - \omega_{B(B)}|$ as well as T_{2A}^{-1} and T_{2B}^{-1} . In this case equation 2.47 simplifies to equation 2.48.

$$G = iB_1 M_z \left(\frac{p_A}{\alpha_A} + \frac{p_B}{\alpha_B} \right) \quad (2.48)$$

Resubstituting for α_A and α_B in the imaginary part of G yields equation 2.49 which simply describes two separate lines of Lorentzian shape with intensities proportional to p_A and p_B .

$$v = \frac{\gamma_e B_1 M_z p_A T_{2A}^{-1}}{T_{2A}^{-2} + (\omega_{B(A)} - \omega)^2} + \frac{\gamma_e B_1 M_z p_B T_{2B}^{-1}}{T_{2B}^{-2} + (\omega_{B(B)} - \omega)^2} \quad (2.49)$$

If the exchange rate increases that k_A and k_B get comparable to T_{2A}^{-1} and T_{2B}^{-1} upon still being smaller than $|\omega_{B(A)} - \omega_{B(B)}|$ one approaches the slow exchange region. In this case one ends up with equation 2.50. There are still two individual Lorentzian lines that are slightly broadened by an amount depending only on the exchange rates k_A and k_B which is key for the line broadening experiments described in chapter 2.6.

$$v = \frac{\gamma_e B_1 M_z p_A (T_{2A}^{-1} + k_A)}{(T_{2A}^{-2} + k_A) + (\omega_{B(A)} - \omega)^2} + \frac{\gamma_e B_1 M_z p_B (T_{2B}^{-1} + k_B)}{(T_{2B}^{-2} + k_B) + (\omega_{B(B)} - \omega)^2} \quad (2.50)$$

As the exchange gets faster and approaches $|\omega_{B(A)} - \omega_{B(B)}|$ which is referred to as intermediate region the lines start additionally to shift towards the centre of the spectrum. The decreasing separation of the lines which finally leads to spectral overlap is given by equation 2.51. Note that here $\omega_{B(A)}^0$ and $\omega_{B(B)}^0$ denote the initial Larmor frequencies of the system without

exchange. In this case equation 2.47 cannot be simplified and is therefore usually solved by computational fitting routines.

$$|\omega_{B(A)} - \omega_{B(B)}| = \sqrt{(\omega_{B(A)}^0 - \omega_{B(B)}^0)^2 - 2 \left(\frac{(k_A + k_B)}{(p_A \gamma_A + p_B \gamma_B)} \right)^2} \quad (2.51)$$

From equation 2.51 it is obvious that the lines will completely overlap if k_A and k_B get much faster than $|\omega_{B(A)} - \omega_{B(B)}|$ at the point presented in equation 2.52.

$$(k_A + k_B) = \frac{(p_A \gamma_A + p_B \gamma_B)(\omega_{B(A)}^0 - \omega_{B(B)}^0)}{\sqrt{2}} \quad (2.52)$$

As soon as k_A and k_B exceed the limit of equation 2.52 the region of fast exchange is reached which leads again to a simplified form of equation 2.47. The resulting single Lorentzian is displayed in equation 2.53 were the variables have been summarized according to equations 2.54 and 2.55.

$$v = \frac{\gamma_e B_1 M_z T_2^{-1}}{T_2^{-2} + (\omega_0 - \omega)^2} \quad (2.53)$$

$$\omega_0 = p_A \omega_A + p_B \omega_B \quad (2.54)$$

$$T_2^{-1} = p_A T_{2A}^{-1} + p_B T_{2B}^{-1} + p_A p_B (\omega_{B(A)} - \omega_{B(B)}) \frac{1}{k_A + k_B} \quad (2.55)$$

This single collapsed line is centred at the average resonance frequency with a linewidth proportional to T_2^{-1} . This quantity now starts to decrease if the exchange gets even faster as displayed in equation 2.55. Similar to the exchange broadening in the slow limit this exchange narrowing can be used to determine kinetics in the fast exchange region. [2.14]

The alternating line width effect is basically arising from the modulation of hyperfine splitting constants by intramolecular dynamics. In this text it will be limited to the slow exchange region, since the Bloch model is not working well in the fast exchange region where the spectrum is an average of two or more interchanging states. In literature there are approximations using the peak-to-peak amplitudes for two state problems, however, a correct description requires to solve the secular terms of a time dependent Hamiltonian. [2.12]

In the slow and intermediate exchange region the spectrum is a superposition of two individual spectra with Lorentzian line shape. Analogue to the homogeneous broadening discussed so far the chemical exchange is added to the transverse magnetization G . The average of G for two interchanging states is given in equation 2.56. Here ω_1 and ω_2 denote the frequency to jump from state to state with an average lifetime τ , D_k the degeneracy of the nuclear spin state and the variables n_{1k} and n_{2k} defined in equation 2.57.

$$\langle G \rangle = -\frac{i\omega_1 D_k (m_{I1} + m_{I2})(4 + n_{1k}\tau + n_{2k}\tau)}{2(n_{1k}n_{2k}\tau + n_{1k}n_{2k})} \quad (2.56)$$

$$n_{1k} = (\omega_1 - \omega_2)^2 \tau / 8 - i(\omega_B^0 - \omega + \delta\omega_{1k}) \quad (2.57)$$

2.6 Application to Self-Exchange Processes

In the study of electron self-exchange the line broadening experiment was introduced in the late 1950s [2.15] and has been mainly focused on electron self-exchange. [2.16] Since the method comes with a nanosecond time resolution it is well suited for this problem. Even though all considerations are equal for proton coupled electron self-exchange as well the following discussion will use the terminology of electron self-exchange.

First of all it is important to visualize the concept of excited spin relaxation by degenerate electron self-exchange. Equation 2.58 displays a simplified electron self-exchange in terms of a chemical reaction equation. The arrows symbolize different nuclear spin configurations which makes the two molecules energetically distinguishable as discussed in chapter 2.2. In the current example the observable free spin is associated with the dot that symbolizes the transferred electron. Even though the overall energy is not changed by this process the energy of the excited spin state is nonetheless.



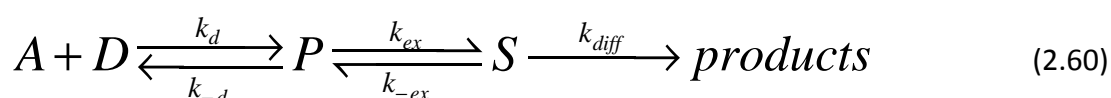
This process is a bimolecular reaction which makes the overall reaction rate dependent on not only the bimolecular rate constant k but also on the concentrations of A^{\bullet} and A . It can, however, be treated as first order kinetics anyways since the concentration of A^{\bullet} will not be changed. Increasing the concentration of A ultimately introduces line broadening by quenching so-to-speak the excited spin states by the electron self-exchange. In the slow exchange region the line width is directly and only dependent on the exchange rates as already pointed out in the context of equation 2.50. All the experimental data was interpreted under this assumption.

The change in linewidth $\Delta B_{pp} - \Delta B_{pp}^0$ with the concentration of A is therefore the experimentally observed quantity. An experimentally observed rate constant k_{obs} as given in equation 2.59 is obtained from the plot of these experimental parameters. This plot is basically a rearrangement of the Heisenberg uncertainty principle in equation 2.18. In order to stay consistent with the experiments γ_e is used in the non SI-unit $s^{-1}G^{-1}$ and the linewidth in the peak-to-peak form. The dimensionless factor p_i attributes for non-detectable exchange in between two molecules of equivalent nuclear spin configurations. It is defined as the n^{th}

degeneration of the i^{th} line normalized by the total number of spin configurations. Strictly speaking each line of different intensity is expected to have a slightly different linewidth but usually it's simply approximated since the changes are within experimental errors.

$$k_{obs} = \frac{\sqrt{3}\pi|\gamma_e|(\Delta B_{pp} - \Delta B_{pp}^0)}{(1 - p_i)[A]} \quad (2.59)$$

In order to translate k_{obs} properly into a rate or electron transfer k_{ET} in the context of Marcus theory the detailed kinetics of the proposed mechanism have to be considered. Equation 2.60 displays the mechanism as a chemical reaction equation. Note that the diffusion from the products to S is defined as the start of a new exchange.



During the experiment the system is in thermal equilibrium so that relation 2.61 is valid as starting equation.

$$k_{obs} * [A] * [D] = k_{diff} * [S] \quad (2.61)$$

In the case of self-exchange the concentrations of P and S will reach a steady state. This is formulated in equations 2.62 and 2.63.

$$\frac{\partial[P]}{\partial t} = 0 = k_d * [A] * [D] + k_{-ex} * [S] - (k_{ex} + k_{-d}) * [P] \quad (2.62)$$

$$\frac{\partial[S]}{\partial t} = 0 = k_{ex} * [P] - (k_{-ex} + k_{diff}) * [S] \quad (2.63)$$

Combining equations 2.61-2.63 leads to a rather complex expression in equation 2.64 for the observed rate.

$$k_{obs} = k_d * \left[1 + \frac{k_{-d}}{k_{ex}} * \left(1 + \frac{k_{-ex}}{k_{diff}} \right) \right]^{-1} \quad (2.64)$$

For an electron transfer with a large driving force k_{ET} is negligible slow. Setting it to zero and substituting for $k_{ex} = K_A k_{ET}$ yields equation 2.65.

$$\frac{1}{k_{ET}} = \frac{1}{k_{obs}} - \frac{1}{k_{diff}} \quad (2.65)$$

For an electron self-exchange it is reasonable to assume $k_{ex} = k_{-ex}$ and $k_{-d} = k_{diff}$ which yields the simple expression in equation 2.66.

$$\frac{1}{k_{ET}} = \frac{1}{k_{obs}} - \frac{2}{k_{diff}} \quad (2.66)$$

In summary all the assumptions lead to simple corrections for diffusion. This is convenient since the rate of diffusion can easily be calculated by the Smoluchowski equation 2.67 from abundantly available parameters. It describes diffusion as simple Brownian motion of

spherical particles. [2.17] N_A denotes the Avogadro constant, r_A and r_D the radii of the reactants and D_A and D_D the Einstein diffusion coefficients which are calculated according to equation 2.68 from the medium's dynamic viscosity η .

$$k_{diff} = 4\pi N_A * (D_A + D_D) * (r_A + r_D) \quad (2.67)$$

$$D_i = \frac{k_B T}{6\pi r_i \eta} \quad (2.68)$$

For a self-exchange process it is reasonable to assume $r_A = r_D$. This conveniently simplifies equation 2.67 to equation 2.69 which is independent from the size of the reactants.

$$k_{diff} = \frac{8RT}{3\eta} \quad (2.69)$$

From the temperature dependence of these experimental rates all the thermodynamic parameters discussed throughout the first chapter of this thesis are accessible. It is, however, important to consider the experimental limitations arising from solubility and thermal stability of the radical. This can be checked by Curie type plots of the double integral versus T^{-1} and the additional determination of signal recovery after cooldown. Moreover, at lower temperatures and resulting high viscosities additional broadening mechanisms such as dipolar interactions might start to interfere. In this case the data is outside the linear regime where equation 2.59 is valid. It can be checked by plotting the line-width versus $T\eta^{-1}$ according to literature. [2.18] The alternating line width effect was discovered in the early 1960ies with the first temperature dependent spectra of the durosemiquinone radical anion where cis-trans isomerism modulates the proton couplings. [2.19] The application to the process of proton exchange was demonstrated from pH-dependent spectra for systems that interchange in between two as well as four states. [2.20]

The data analysis is rather straight forward, since the exchange is usually obtained directly from the simulations in units of frequency. Further the diffusion correction for bimolecular processes from equations 2.65 and 2.66 is unnecessary since even if one deals with a bimolecular process like proton exchange with the medium the reactant is always in contact.

2.7 ENDOR

The abbreviation ENDOR stands for Electron Nuclear Double Resonance. It is a coupled experimental technique that basically uses an ESR Spectrometer to detect NMR transitions. The first report of this type of experiment dates to the mid 1950ies. [2.21] A general overview of all the possible applications is given in various textbooks. [2.22] In the context of this thesis it was used to obtain experimental hyperfine splitting constants if they were not accessible

from the conventional ESR spectrum. As already discussed in chapter 2.4 all magnetically active nuclei couple to one single electron spin which results in a multitude of often unresolved lines. In NMR, however, each nucleus has its own gyromagnetic ratio and therefore a distinct Larmor frequency. In principle hyperfine splitting constants can be obtained from a conventional NMR spectrum of a radical. Unfortunately strong dipolar interactions often broadens these signals strongly for a significant amount of radicals in a way that makes them indistinguishable from the noise.

Figure 2-7 illustrates the concept of an ENDOR experiment for the simplest system possible: a hydrogen atom with $S = \frac{1}{2}$ and $I = \frac{1}{2}$. The four boxes illustrate the spin states with a population according to the colouration. Vertical lines correspond to ESR transitions, horizontal lines to NMR transitions and the dashed lines to so-called cross relaxations.

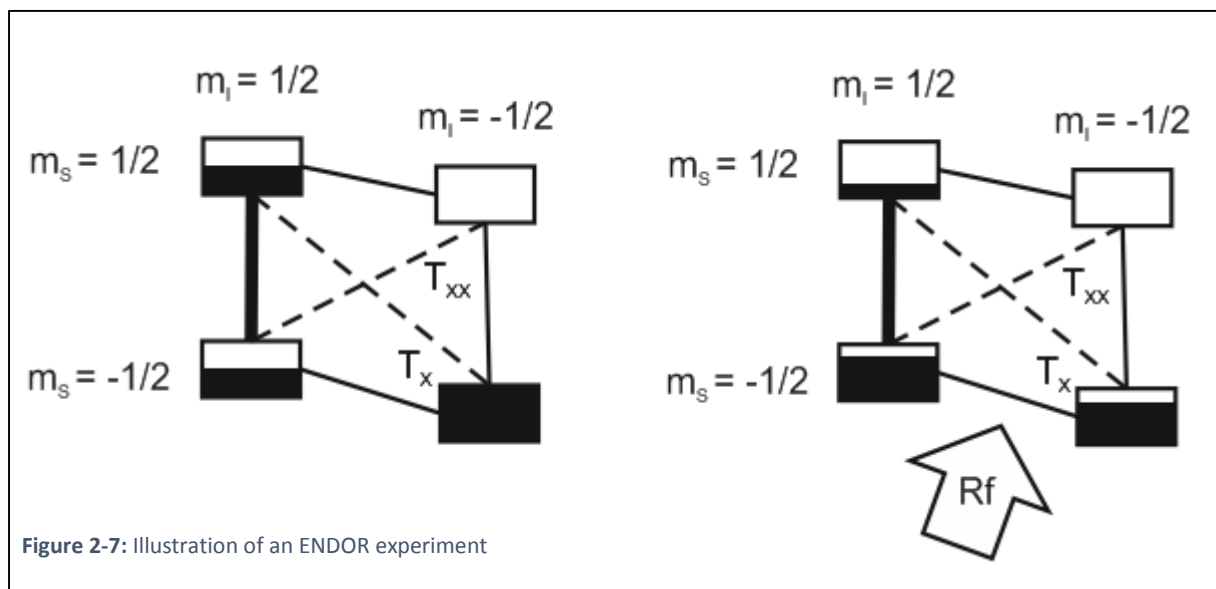


Figure 2-7: Illustration of an ENDOR experiment

On the left side the situation is displayed for a saturated ESR transition. It means that the corresponding spin states are equally populated so that the absorption signal vanishes. As soon as the population of these states is altered by applying an intense radiofrequency R_f to induce coupled NMR transitions the absorption signal will reappear as displayed on the right side.

If the relaxation would only be dependent on τ_1 which is compensated by the saturation no steady ENDOR signal could be observed. However, there are additional exergonic two-quantum processes T_x and T_{xx} which are referred to as cross-relaxation. They are both related to the rotational correlation time τ_R which is displayed in equation 2.70. It is dependent on the dynamic viscosity η and the effective volume V_{eff} which is usually approximated by a sphere with an average radius of the molecule. All these processes are highly dependent on

temperature in different relations. In fact temperature is the most crucial parameter for the ENDOR experiment.

$$\tau_R = V_{eff} \frac{\eta}{k_B T} \quad (2.70)$$

In order to interpret the ENDOR spectrum which displays the reappearing absorption versus the radio frequency in MHz the simplified Hamiltonian in equation 2.16 needs to be reconsidered. Its eigenvalues for a system with $S = \frac{1}{2}$ yield the two energy levels arising from the electron Zeeman splitting in equations 2.71 and 2.72.

$$E_{(m_s = \frac{1}{2})} = g_e \mu_B B + \left| \frac{A}{2} - g_n \mu_n B \right| m_I \quad (2.71)$$

$$E_{(m_s = -\frac{1}{2})} = g_e \mu_B B - \left| \frac{A}{2} + g_n \mu_n B \right| m_I \quad (2.72)$$

Applying NMR selection rules of $\Delta m_s = 0$ and $\Delta m_I = \pm 1$ one can observe two transitions with the frequencies ν_1 and ν_2 within each of this further split Zeeman level. Equation 2.73 therefore presents ν_1 in the Zeeman level of equation 2.71 as difference of both values of m_I and 2.74 the frequency ν_2 in the level of equation 2.72 respectively.

$$\nu_1 = \left| \frac{A}{2} - g_n \mu_n B \right| h^{-1} \quad (2.73)$$

$$\nu_2 = \left| \frac{A}{2} + g_n \mu_n B \right| h^{-1} \quad (2.74)$$

The difference of ν_1 and ν_2 thus equals $A h^{-1}$ which means that the hyperfine splitting constant is the direct readout of the distances of two corresponding signals in the spectrum.

2.8 References

- [2.1] P. Zeeman, Verh. Phys. Ges. Berlin 7, 128 (1896)
- [2.2] a) O. Stern and W. Gerlach, Z. Phys. 9, 349 (1922)
b) G.E. Uhlenbeck and S. Goudsmith, Naturwissenschaften 13, 953 (1925)
- [2.3] E. Zavoisky, J. Phys. USSR 9, 211 (1945)
- [2.4] R.L. Cumberow and D. Halliday, Phys. Rev. 10, 433 (1946)
- [2.5] a) F. Bloch, Phys. Rev. 70, 460 (1946)
b) F. Bloch, W.W. Hansen and M. Packard, Phys. Rev. 70, 474 (1946)
c) E.M. Purcell, H.C. Torrey, and R.V. Pound, Phys. Rev. 69, 37 (1946)
- [2.6] F. Gerson and W. Huber, ESR Spectroscopy of Organic Radicals, VCH (1988)
- [2.7] G. Jeschke, Einführung in die ESR-Spektroskopie, VO-Skript Uni Konstanz (1998)
- [2.8] J.A. Weil and J.R. Bolton, EPR: Theory and Practical Applications 2nd Ed., Wiley (2007)
- [2.9] K. Scheffler and H.B. Stegmann, Elektronenspinresonanz, Springer (1970)
- [2.10] a) C.P. Poole Jr., ESR – A Compreh. Treatise on Experimental Techniques, Wiley (1967)
b) T.K. Ishii, Handbook of Microwave Technology Vol. 2, Academic Press (1995)
- [2.11] G.R. Eaton, S.S. Eaton, D.P. Barr and R.T. Weber, Quantitative EPR, Springer (2010)
- [2.12] A. Hudson and G.R. Luckhurst, Chem. Rev. 69, 191 (1968)
- [2.13] a) A.G. Redfield, IBM J. Res. Develop. 1, 19 (1957)
b) A.G. Redfield, Adv. Mag. Res. 1, 1 (1965)
- [2.14] a) L.H. Piette and W.A. Anderson, J. Chem. Phys. 30, 899 (1959)
b) V.G. Koshechko, V.E. Titov and V.D. Pokhodenko, Teor. Eksp. Khim. 19, 161 (1983)
- [2.15] R.L. Ward and S.I. Weissmann, J. Am. Chem. Soc. 79, 2086 (1957)
- [2.16] G. Grampp, Spectrochim. Acta A 54, 2349 (1998)
- [2.17] M. Smoluchowski, Ann. Phys. 326, 756 (1906)
- [2.18] B. Berner and D. Kivelson, J. Phys. Chem. 83, 1406 (1979)
- [2.19] J.R. Bolton and A Carrington, Mol. Phys. 5, 161 (1962)
- [2.20] a) H. Fischer, Mol. Phys. 9, 149 (1965)
b) I. Yamakazi and L.H. Piette, J. Am. Chem. Soc. 87, 986 (1965)
- [2.21] G. Feher, Phys. Rev. 103, 834 (1956)
- [2.22] H. Kurreck, B. Kirste and W. Lubitz, ENDOR Spectroscopy of Radicals in Solution, VCH (1988)

3. Methods and Instruments

3.1 Solvent Purification

For ESR experiments all organic solvents were routinely dried over corresponding molecular sieves in preparative columns under nitrogen atmosphere. The standard volume used was about half a litre which takes about 12 h. The slow flow rate guarantees best water adsorption. Further the bottom flask contained additional sieve material to increase the performance.

Directly after drying all solvents were distilled under corresponding pressure conditions. At normal pressure distillation was performed under nitrogen atmosphere. The final solvent was stored in Schlenk flasks under nitrogen atmosphere in a desiccator. If necessary light was blocked upon storage by dark fabric.

Prior to use smaller amounts of the solvent were transferred – every syringe and pipette was flushed thrice with nitrogen atmosphere directly before use – upon using Schlenk techniques to degas them. This was done by carefully purging the solvent with dry nitrogen gas – using either a glass frit, glass tubes or blunt cannula - for about 15 min per 50 ml. On one hand this procedure makes final removal of oxygen easier and on the other it avoids radical decay by reactions with oxygen.

Ionic liquids on the other hand were purchased from Io-Li-Tec (Germany) since they give very detailed analytic information. We dried them for at least 36 h at 310 K and high vacuum. This could be achieved by a special oil diffusion pump from Leybold. (Germany) The dried ILs were stored and handled under nitrogen atmosphere using Schlenk techniques.

3.2 Sample Preparation

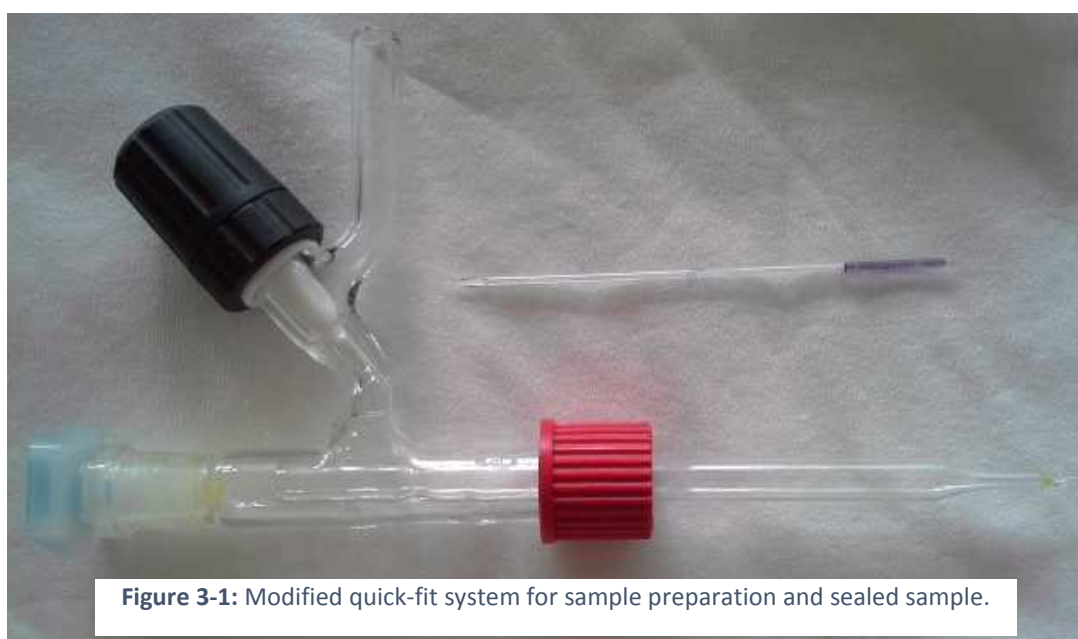
Dependent on the radical's stability two types of sample preparation are distinguished. Stable radicals were sealed under vacuum, whereas for the in-situ generated ones – which was done in continuous flow – they differ for electrochemical and photochemical generation.

From stable radicals a few millilitres of a stock solution of about 0.5 mM radical was prepared under nitrogen atmosphere. It was further divided in several points of 1 ml and different amounts of neutral substance were added. In order to achieve proper solvation we applied either ultrasonic or magnetic stirring.

Figure 3-1 displays a final sealed sample as well as the apparatus used for preparing it. The Apparatus is basically a small pipe with a gas connection to the Schlenk system and a gas tight quick-fit system to hold a Pasteur pipette. The pipette is sealed at its tip over a flame and

mounted. Inert atmosphere is established by three consecutive cycles of vacuum and nitrogen. Then about 40 μl of sample solution are transferred inside the pipette. If the solution does not run to the bottom by itself, rigorous shaking is applied. Then oxygen is removed by at least three consecutive freeze-pump-thaw cycles using a small Dewar of liquid nitrogen. It might be necessary to shake the solution again after thawing the first two times.

Finally the sample is frozen again and sealed under vacuum. Depending on the radical it is stable from hours to months. At least three individual samples are usually prepared from one solution in order to assure reproducibility. The sealed capillaries are put into a standard ESR-tube in order to measure them.



For electrochemical radical generation at least 15 ml of sample solution were required. Firstly a stock of solvent with supporting electrolyte was prepared and divided into a series of concentrations of neutral substance. Depending on how hygroscopic the solvent or substance is, this can even be done under standard atmosphere. Oxygen was removed inside the flow system itself which is explained in chapter 3.4. The same applies to photochemical radical generation, with the one small difference, that no supporting electrolyte is required.

3.3 Spectrometer Setup

All ESR experiments were performed with an ELEXSYS E-500 spectrometer from Bruker. It operates at X-Band with a modulation frequency of 100 KHz.

Additionally it is equipped with an ER4131VT digital temperature control unit. This unit uses liquid nitrogen as heat carrier which limits the temperature window to 160 – 380 K. It works with a precision of ± 0.1 K if one works at one temperature and with ± 0.5 K if one uses the

automatic temperature ramp option. The temperature is measured by a Pt-100 element directly below the sample for sealed ones and on the surface of the capillary in the flow system.

All but the photochemical systems were measured in a cylindrical HSW10100 high resolution resonator which is optimized for cylindrical sample geometries. For the photochemical experiments we used a 4104 OR-R 9902 shot-through Resonator from Bruker. It was equipped with a flat cell.

3.4 The Flow System

Figure 3-2 displays a sketch drawing of the system in its final configuration which will be explained in the direction of operation. In the beginning the entire system is purged with slight overpressure of dry nitrogen at the upper stop-cock V_1 of the storage flask A while it is closed at the top. This overpressure is applied continuously for the entire process.

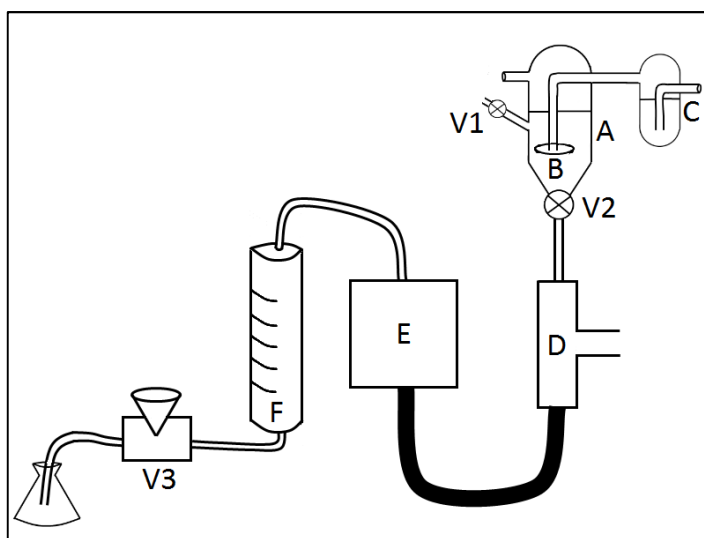


Figure 3-2: Sketch of the flow system

During degassing it ensures inert atmosphere and during operation it is required to get the solution through the entire system.

After 10 min of purging the lower stop-cock V_2 is closed, the solution inserted and degassed through the glass frit B. In order to eliminate concentration changes through solvent evaporation in the nitrogen stream it is saturated in the flask C before. For a volume of 15 ml degassing is completed after 15 min. Then the glass frit B is exchanged for a secured plug and the lower valve V_2 is opened.

All tubing is made from special Teflon with low oxygen permeability. Starting from the T-fitting D the tubing to the resonator is additionally mantled with a black – only necessary for photo-sensible systems – silicon tube. In between these two tubes a constant stream of dry nitrogen is flowing in order to eliminate the remaining oxygen diffusion.

After passing through the resonator region E – how the setups to generate radicals operate is explained in the following chapters – the flow rate is measured at point F with a shielded GF-2060 flowmeter from Gilmont Instruments. They are usually in a range below 1 ml min⁻¹.

The flow rate itself is controlled with the manually operated special conical screw-valve V3. It is made from Teflon and has an extremely fine thread to ensure small changes in the tube diameter. It has to be fine since the flow rate is dependent on the radius by r⁴ according to the law of Hagen-Poiseuille.

For the work on ionic liquids flask A was changed to a smaller one with a volume of 4 ml without a valve at the bottom. This flask was placed directly in front of the cavity in order to reduce the length of tubing. Samples were degassed through a sawed off Pasteur pipette mounted directly on the nitrogen line since evaporation is not an issue. This system enables to work with sample volumes smaller than 0.5 ml with an additional option for temperature control. For this the flow was just stopped when the capillary in the cavity was filled. Thermal equilibrium is usually reached after 20 min.

3.5 The Electrochemical Setup

The system is designed to produce radicals under galvanostatic conditions. Before going in technical details the main challenges are presented in terms of Faraday's law. It is displayed in equation 3.1 in a form that reflects the experimental situation.

$$[R^\bullet] = \frac{1}{nF} * |I| * \frac{1}{u} \quad (3.1)$$

Here [R[•]] denotes the produced concentration of radical in [mol], n the number of transferred electrons per molecule, F the Faraday constant with 96458 [C mol⁻¹], I the exchange current in [A] and u the flow rate (dV/dt). Even though u is usually measured in [ml min⁻¹] in equation 3.1 uses it in l s⁻¹ units. The conversion factor for u to be the measured value is 60000.

For the line broadening experiment the radical concentration is the most crucial variable. Unfortunately it is dependent on the two variables I and u which have to be measured and controlled carefully during operation. In order to minimize this source of error we kept u fixed while changing the current by regulating the potential. In addition to this the concentration of an unstable radical itself is a function of time since it decays at a specific rate. This makes the choice of u even more crucial since fast flow is favourable for little radical decay, however, disadvantageous for the electrochemical radical generation. Therefore one must not just measure I and u to calculate [R[•]] which was always checked from the double integrals of each

spectrum. A standard error of 5% is reasonably assumed on which arises from integrating the signal with the background noise.

Figure 3-3 displays a sketch of the electrochemical system. Only the central reaction cell G is mounted inside the magnet which corresponds to position E in figure 3-2.

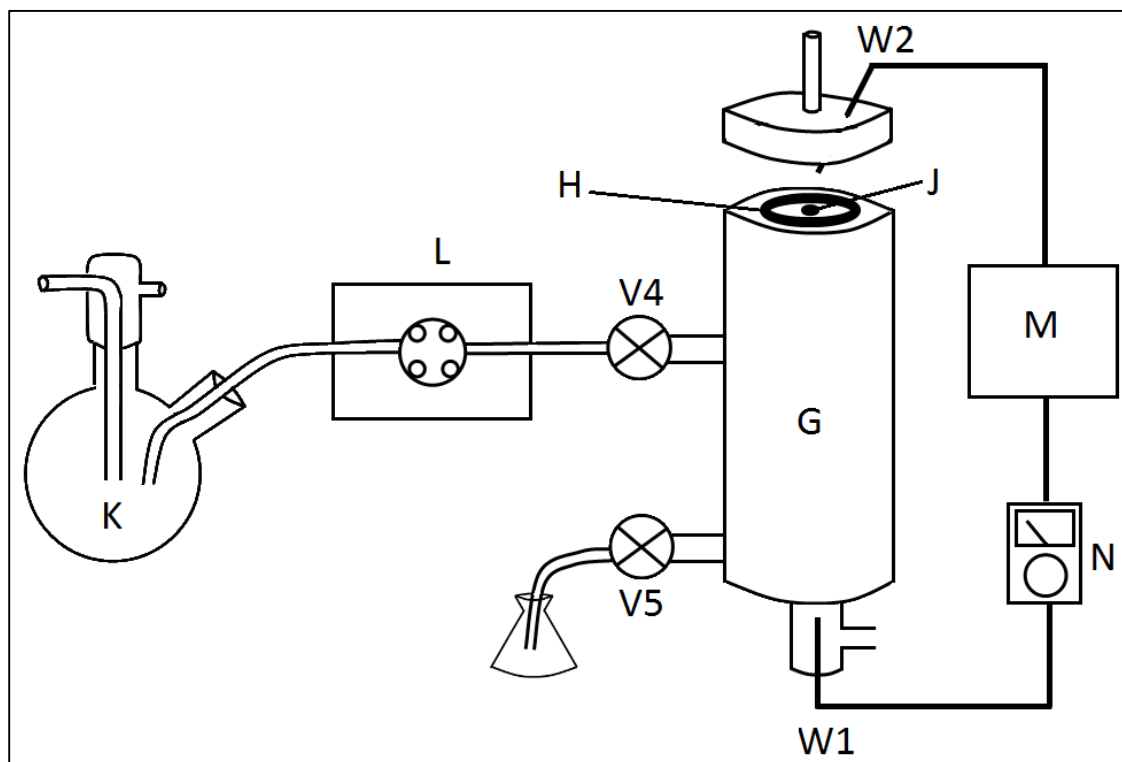


Figure 3-3: Sketch of the electrochemical system.

The reaction cell G is a simple cylindrical two electrode setup. The counter electrode H is made from a flexible carbon mesh and contacted via the tungsten wire W_1 , while the working electrode J is made from a carbon fibre and contacted by wire W_2 . In between the two electrodes a porous Teflon cylinder is placed to separate the two half-cells.

The sample solution fills the electrochemical cell from the bottom up and runs directly in a quartz capillary. It has an outer diameter of 4 mm and an inner diameter of 0.8 mm and is placed through the resonator. The short tube from the cell to the capillary is black in order to work with photosensitive radicals as well.

The outer electrochemical half-cell is filled with a solution of supporting electrolyte. This solution is degassed in flask K and transported with a peristaltic pump L. During operation the outer half-cell has to be closed by valves V_4 and V_5 . Otherwise the pressure from the flow system would press the sample solution through the Teflon separator.

Finally a home-built galvanostat M is used. It operates in a potential range of ± 10 V which is manually adjusted. During operation we measured the exchange current by a conventional voltmeter N which was permanently integrated in the circuit.

All experiments were performed by the following routine:

- 1) About 500 ml of solvent containing supporting electrolyte were prepared. Meanwhile the entire flow system is purged with dry nitrogen gas.
- 2) 100 ml of the supporting electrolyte solution are degassed for 25 min in flask K. Without stopping the nitrogen flow in flask K the whole outer half-cell was filled with pump L. When the pumped solution reached the waste V_3 and V_4 were closed and the pump is switched off.
- 3) The targeted constant radical concentration is dissolved in another 500 ml of electrolyte solution and degassed in flask A under inert atmosphere for 30 min.
- 4) After degassing is completed frit B is exchanged for a plug
- 5) The galvanostat M is set to a small potential and switched on
- 6) Valves V_3 and V_2 are opened until the solution has filled the capillary in the cavity. Then the flow rate is reduced with valve V_3 .
- 7) Potential and flow rate were optimized to observe maximum ESR signal which is checked by the double integrals. At this point quantitative conversion is assumed. If maximum signal is observed the position of valve V_3 was kept constant.
- 8) After acquiring as many spectra of constant double integral as possible the flow system is flushed with methanol.
- 9) All further samples with a higher concentration of neutral substance can be done with smaller volumes down to 10 ml. Proceed as described before with one important difference: Keep the flow rate constant!
- 10) After completing one series of experiments all valves are opened to empty the system. Then it is cleaned by pumping methanol through all components and dried with a stream of dry nitrogen gas.

3.6 The Photochemical Setup

The light source was a 500W Mercury-vapour lamp from Osram which is equipped with a focusing lens in housing. The IR-radiation was filtered by a 20 cm water pass which is integrated in the lamps cooling circuit.

It was operated similarly to the electrochemical system, even though the flow rate was changed to keep the produced radical concentration constant.

3.6 Density and Viscosity

A modified version of the L-Dens density transmitter from Anton Paar (Graz, Austria) was used. An external thermal bath (278 – 360 K) where the water is circulated and a data transfer option via RS232 were added. Over the full range we determined the experimental error to be $\pm 0.0002 \text{ g ml}^{-1}$ (from 0.5000 to 2.0000 g ml^{-1}) with a precision of $\pm 0.1 \text{ K}$ for the temperature. The temperature dependence of the density ρ was routinely described by the linear approach given in equation 3.2.

$$\rho_T = a * T + b \quad (3.2)$$

Viscosities were determined with Ubbelohde viscosimeters operated under the DIN 51562/2 requirements. We connected it to the same external thermal bath as the density transmitter. For organic solvents we used a 50103/0c capillary from Schott Company (Germany) and fitted the data via an Arrhenius type equation 3.3.

$$\eta_T = A + \exp\left(\frac{H_\eta}{RT}\right) \quad (3.3)$$

When working with ionic liquids we used the 53623/IIc micro-capillary from SI Analytics GmbH (Mainz, Germany) and fitted the data via the Vogel-Fulcher-Tallmann equation 3.4.

$$\eta_T = A + \exp\left(\frac{B}{T - T_0}\right) \quad (3.4)$$

4. Electron Self-Exchange of ZnTPP and its corresponding π -Radical Cation

4.1 Introduction

In a way metal porphyrins could be called nature's electron transfer system of choice. Throughout the entire known biosphere metal porphyrins and their corresponding π -radical cations as well as the anions are known to play a major part in vitally important electron transfer processes such as photosynthesis or the activation of oxygen in mammal's blood.

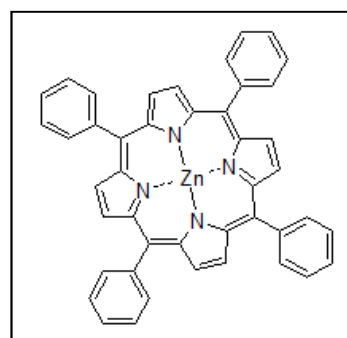


Figure 4-1: Structure of ZnTPP

[4.1] This circumstance caused decades of intensive research in

order to exploit these systems for e.g. artificial photosynthesis [4.2] or the in situ production of singlet oxygen. [4.3]

It is remarkable that at the point this project was started only one study on electron self-exchange kinetics of metal porphyrins was reported in literature. The self-exchange of two complexes zinc-5,10,15,20-tetraphenylporphyrine (in the following ZnTPP – structure displayed in Figure 4-1) and 5,10,15,20-tetra-4-tert-butylphenylporphyrine with their corresponding π -radical cations was investigated in three organic solvents at different temperatures. From the temperature data this study reported negative activation energies since the lines got broader with decreasing temperature. Further the rates appeared to not follow the general dependence on the Pekar factor which was not discussed at all. [4.4]

In previous work we showed for ZnTPP that the method of this study can't be reproduced since the reactants are either not soluble or one does not yield a pure radical. A strong indication for this was that the hyperfine splitting constants of the published study did not fit to our experimental spectra. The first problem was overcome by electro-generating the radical in-situ using our electrochemical flow system. Figure 4-2 shows the significant change in colour upon

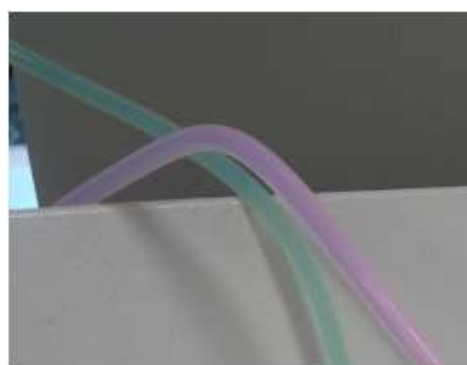


Figure 4-2: Solution of ZnTPP (pink) and electro-generated ZnTPP^{•+} (green) during experimental operation

electrochemical conversion. Further we solved the hyperfine structure by ENDOR experiments and gave an alternative explanation for the broadened lines in terms of dipolar coupling. [4.5] In this work we reinvestigated the electron self-exchange kinetics of the ZnTPP/ZnTPP^{•+} system in three polar organic solvents – butyronitrile, ethyl acetate and propylene carbonate – at room temperature with the electrochemical system at 294 K. We could not find a deviation from Marcus Theory so far and the results were published. [4.6]

4.2 Experimental

ZnTPP was synthesized according to the procedure of Adler et al. [4.7] in refluxing DMF (Roth 99,8 %) from 5,10,15,20-tetraphenyl-21H,23H-porphyrine (Sigma Aldrich 99 %) and an excess of dry zinc-(II)-chloride (Merck 98% p.a.). Reaction progress was monitored by either UV-VIS spectroscopy (increasing band at 550 nm) as described in literature or TLC on silica gel 60. Using a mobile phase of chloroform: n-heptane = 1:3 and UV detection one obtains R_f-values of 0.147 for ZnTPP and 0.256 for H₂TPP. The remaining salt was removed quantitatively by column-chromatography with a neutral aluminium oxide column and chloroform as mobile phase. The solvent was finally evaporated under reduced pressure in order to obtain a pure product. ¹H NMR (DCCl₃, 200 MHz): δ 7.79 (m, 12H), 8.25 (m, 8H), 8.99 (s, 8H).

The supporting electrolyte tetrabutylammonium tetrafluoroborate (Fluka pure) was dried at 350 K under vacuum for at least 12 h and stored under nitrogen atmosphere.

Samples were prepared using Schlenk techniques. For each solvent a stock solution containing 2 mM supporting electrolyte was prepared. From the stock five samples with different concentrations of the neutral ZnTPP were prepared in a concentration range of $2 \cdot 10^{-4}$ – $1 \cdot 10^{-3}$ M to a final volume of 15 ml per sample.

The electrochemical flow system was used to perform the line broadening experiments at a temperature of 294 K. Flow rate and exchange current were optimized to generate a constant radical concentration of $2 \cdot 10^{-4}$ M. Flow rates were about 1.5 ml min⁻¹ and the exchange currents smaller than 10 mA. Spectra were recorded with 100 kHz modulation and a modulation amplitude of 0.5 G. From one sample up to 10 spectra can easily be recorded to ensure reproducibility. The final radical concentration was checked by double integration. Only deviations of less than 7 % on the double integral were tolerated.

4.3 Results and Discussion

Figure 4-3 displays an exemplary experimental spectrum of ZnTPP/ZnTPP^{•+} 4/1 in butyronitrile and a corresponding simulation. The spectra were fitted by a simplex-algorithm in winsim2002 from Bruker with 4N 1.5 G and 8H 0.25 G as hyperfine splitting constants. Other

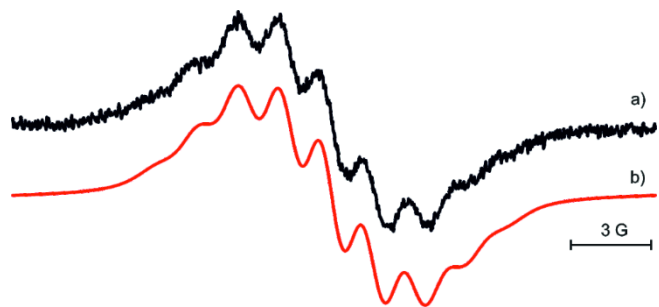


Figure 4-3: Spectrum of 0.2 mM ZnTPP^{•+} with a fourfold excess of ZnTPP at 294 K in butyronitrile (a) and corresponding simulation (b)

software with more complex algorithms failed with these spectra. The problem came from the considerable noise and unresolved hyperfine structure from the protons. Therefore the broadening is hardly visible to the bare eye. Going to larger concentrations of either the radical or the neutral ZnTPP would lead to more visible changes, however, solubility limits the concentration range.

Figure 4-4 displays a plot of the obtained peak-to-peak line widths ΔB_{pp} versus the concentration of neutral ZnTPP. Each point is calculated as the average of at least 5 individual measurements. The error bars correspond to the standard deviation of the measured datapoints.

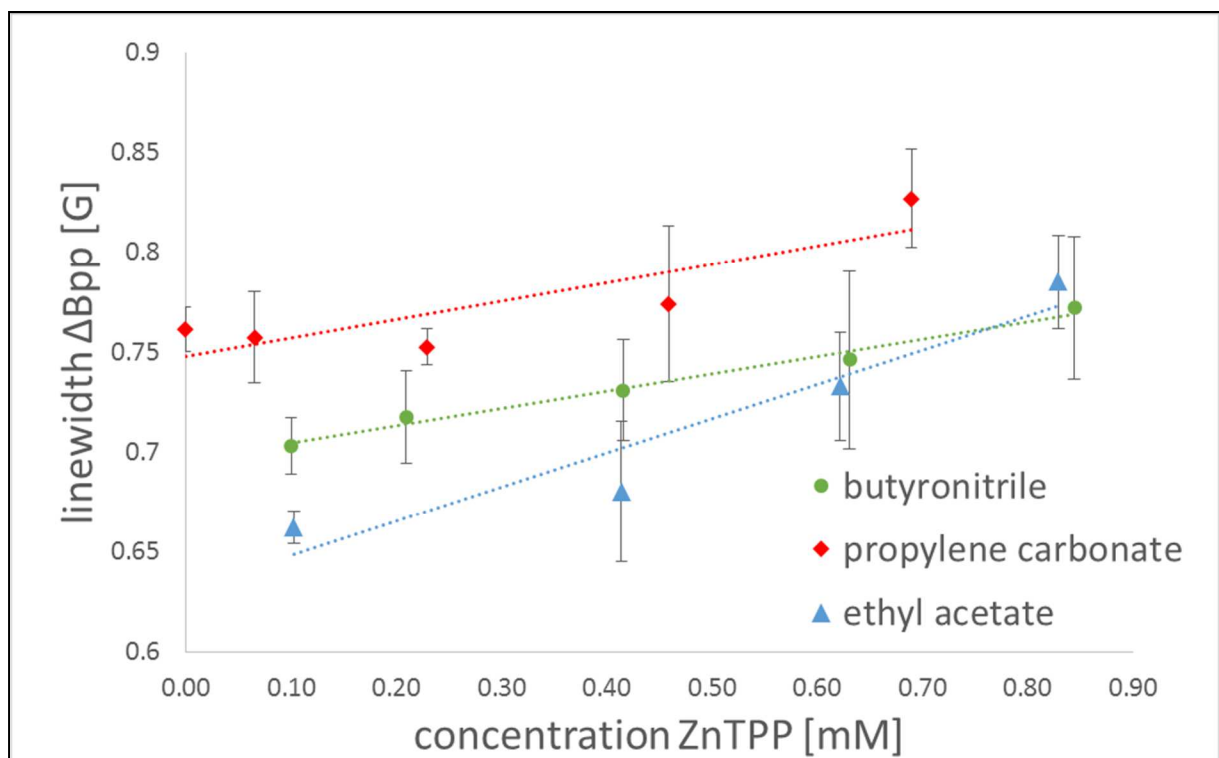


Figure 4-4: Plot of linewidth versus concentration of neutral ZnTPP

The slope was interpreted according to equation 2.59 in chapter 2. Even though the ESR signals are not base-line separated the assumption of slow-exchange is a reasonable compromise due

to the low concentrations that were used. Further we estimated the statistical factor p_i to be 1/9. The relatively large error bars are an overall estimate – 30 % are usually assumed to the method itself – that include additionally the horizontal error on the actual radical concentration. This issue is related to the in-situ generation of radicals and was already addressed in chapter 3.5 in detail.

All obtained, calculated and corrected rates are summarized in table 4-1. Additionally literature values for the dynamic viscosity η and the Pekar factor γ for each solvent are displayed.

Table 4-1: Summary of rates in 10^9 [$M^{-1} s^{-1}$] and relevant solvent parameters

Solvent	η [cP]	γ	k_{diff}	k_{obs}	k_{ET}
butyronitrile	0.58 ^[4.8]	0.483 ^[4.9]	11.4	1.5	2.0
ethyl acetate	0.49 ^[4.8]	0.318 ^[4.10]	13.4	3.1	5.7
propylene carbonate	2.77 ^[4.9]	0.480 ^[4.11]	2.37	1.6	1.6

The experimental rates k_{obs} were corrected for diffusion by equation 2.64 as described in chapter 2. In the comparably high viscous propylene carbonate, however, this correction lead to a seemingly negative value for k_{ET} . Therefore we assume total diffusion control for this reaction by assuming $k_{obs} = k_{ET}$ for this solvent.

Our rates are in the same order of magnitude as the ones from previous literature. [4.4] If one has a closer look at the data, however, there are two strong arguments that the system behaves as predicted from Marcus Theory. They exclusively relate to the other sphere reorganization energy which was discussed in chapter 1.4. Firstly we observe the fastest rate in the least polar solvent. Ethyl acetate has a 35 % smaller Pekar factor compared to the other solvents and the electron self-exchange rate is observed about 3 times faster. Secondly the rates in the other two solvents are within experimental error basically the same even though propylene carbonate is about 6 times more viscous than butyronitrile. This proves that in fact other sphere reorganization mainly determines the rate instead of mass transport.

Finally, we tried to include more solvents within the limitations of the method. Besides the electrochemical window of the solvent, the solubility of supporting electrolytes is the main restriction additional to the solubility of the reactants themselves. Unfortunately we failed to get sufficiently intense signals in dimethylformamide and propionitrile. In 1,2-dichlorobenzene we were unable to observe a clear trend. Therefore we did not process this data any further.

4.4 Outlook and Conclusion

We successfully measured electron self-exchange rates of the ZnTPP/ZnTPP^{•+} redox couple with our electrochemical setup. We are convinced that despite the considerable experimental error our method provides more reliable data. On one hand there are less electrochemically active species present in the sample and on the other the flow compensates for chemical radical decay.

Further we did not find any deviation from Marcus Theory within the experimental range of solvent polarity. This also showed that this predicted trend is quite robust against bias from the solvent's viscosity. However, this must be confirmed by going to less polar solvents which would require the use of special supporting electrolytes. These are difficult to handle and rather expensive. Moreover, they are known to have a different impact on the solvent's viscosity which was neglected in the analysis of this data. [4.12]

Finally, it is important to state that the ZnTPP/ZnTPP^{•+} system is not a convenient system for line broadening experiments. Especially the large number of unresolved hyperfine splitting from the protons superimpose a significant bias on the interpretation of experimental spectra. With an X-band spectrometer this problem cannot be overcome. Therefore it might be more interesting to go to different methods such as CIDEP to study photo-induced electron transfer dynamics upon probing the signals of acceptors such as quinones. This has been shown in principle already. However, this work focuses on one solvent only and was not interpreted in terms of Marcus theory. [4.13]

4.5 References

- [4.1] D. Dolphin and R.H. Felton, *Acc. Chem. Res.* 7, 26 (1974)
- [4.2] G. Bottari, O. Trukhina, M. Ince and T. Torres, *Coord. Chem. Rev.* 256, 2453 (2012)
- [4.3] P. Maillard, P. Krausz and C. Giannotti, *J. Organomet. Chem.* 197, 285, 290 (1980)
- [4.4] S. Fukuzumi, T. Hasobe, Y. Endo, K. Ohkubo and H. Imahori, *J. Porphyrins Phtalocyanines* 7, 328 (2003)
- [4.5] J. Bächle, Master Thesis, Graz University of Technology (2014)
- [4.6] J. Bächle, B. Mladenova and G. Grampp, *Chem. Phys. Lett.* 620, 35 (2015)
- [4.7] A.D. Adler, F.R. Longo, F. Kampas and J. Kim, *J. Inorg. Nucl. Chem.* 32, 2443 (1970)
- [4.8] J.A. Riddick, W.B. Bunger, T.K. Sakano, *Organic Solvents – Physical Properties and Methods of Purification*, Wiley New York (1986)
- [4.9] Y. Marcus, *The Properties of Solvents*, Wiley (1998)
- [4.10] R.M. Shrike, A. Chaudhari, N.M. More, P.B.J. Patil, *Mol. Liquids* 94, 27 (2001)
- [4.11] J. Barthel, R. Buchner, C.G. Hölzl and M. Münsterer, *Z. Phys. Chem.* 214, 1213 (2000)
- [4.12] G. Jones and M. Dole, *J. Am. Chem. Soc.* 51, 2950 (1929)
- [4.13] J. Schlüpmann, K.M. Shalikhov, M. Plato, P. Jaegermann, F. Lenzian and K. Möbius, *Appl. Mag. Res.* 2, 117 (1991)

5. Electron Self-Exchange of TTF/TTF^{•+} in a Binary Mixture of Ionic Liquids

5.1 Introduction

An ionic liquid (IL) is a salt with a melting point below room temperature. The history of this class of substances depends strongly on the author. However, most agree that it started with the so-called red oil in the middle of the 19th century and remained relatively unnoticed until the 1960s. This was the time when new electrolytes for thermal batteries should replace the used molten LiCl/KCl salt. [5.1]

In fact ionic liquids have remarkable properties such as being inflammable and having a high vapour pressure, a large electrochemical window and good electric conductivity. Moreover, they are able to dissolve organic and inorganic substances well. Therefore the field of applications in synthesis and technology has become rather wide. [5.2] Moreover, it is quite remarkable that there is still intensive research to use them as electrolytes in battery technology – the topic where the interest started – such as state of the art lithium ion batteries. [5.3]

Besides the advantages there are some major draw backs with this type of materials. First of all impurities such as ions, unconverted reactants and water lead to varying properties. Further they have comparably high viscosities that are quite strongly dependent on temperature. For commercial ILs one finds hence activation barriers for mass transport H_{η} around 30 kJ mol⁻¹. [5.4]

Even though they are already used as electrolytes, there is still no unified and comprehensive theory available to describe ET in ILs. Therefore this work is a follow up project to the work of a previous PhD-student in our group who was studying electron self-exchange in ILs. [5.5] Besides, the problem arising from the fact that quantities like the Pekar factor or the longitudinal relaxation time is ill defined for ILs the large activation energy of the mass transport can cause problems.

The last problem was first encountered and published for the redox couple of tetrathiafulvalene and the corresponding radical cation. (TTF/TTF^{•+}) [5.6] Figure 5-2 displays the structure of TTF. There the experimental activation barriers for mass transport and

electron self-exchange were equivalent. Therefore total diffusion control for this process was concluded so that H_{η} was simply added to the activation barriers of every electron self-exchange in ILs. [5.7]

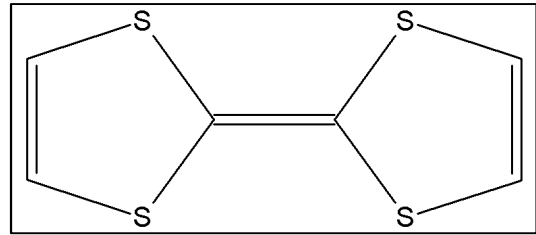


Figure 5-2: Structure of TTF

The goal was to develop an experimental routine that is able to eliminate the temperature dependence of the viscosity. Binary mixtures of two ILs – liquids 1-ethyl-3-methyl-imidazolium and tri-octyl-methyl-ammonium bis-trifluoromethylsulfonyl-imide (EMIM NTf₂ and OMA NTf₂) – were prepared and characterized where just the molar fractions of the two components determine the viscosity. With this one can take the room temperature viscosity of the low viscous component and find higher temperatures where each of the more viscous mixtures has the same viscosity. If one now performs kinetic experiments in every mixture at this specific temperature, one measures a temperature dependent rate at constant viscosity. This enables the experimental separation of the activation of mass transport from the activation of the studied process.

This chapter mainly focuses on the process of finding an adequate mixture, developing a protocol for the characterization and checking the general applicability by reinvestigating the electron self-exchange of TTF/TTF^{•+}.

5.2 Theoretical Considerations

The major challenge is to find two ILs with the right set of properties. It is necessary to consider the following points:

- 1.) Usually anion influences the ILs viscosity stronger than the cation. Therefore it is not recommended to mix different types of anions. [5.10]
- 2.) It is important to have cations that do not interact strongly with each other. It has been shown that e.g. hydrogen bonding can lead to rather complicated behaviour of mixtures. [5.11]
- 3.) The final viscosity at which the experiment is finally conducted should be as small as possible in order to decrease errors from the sample preparation.
- 4.) The accessible temperature window should exceed a range of 40 K in order to get reasonable activation parameters.

Since EMIM NTF₂ is known to have a comparably low dynamic viscosity at room temperature of about 30 mPa s the focus was set on ILs with the TTF⁻ anion. Unfortunately most of these ILs are in a similar range of viscosity which is visualized in figure 5-2 for literature data.

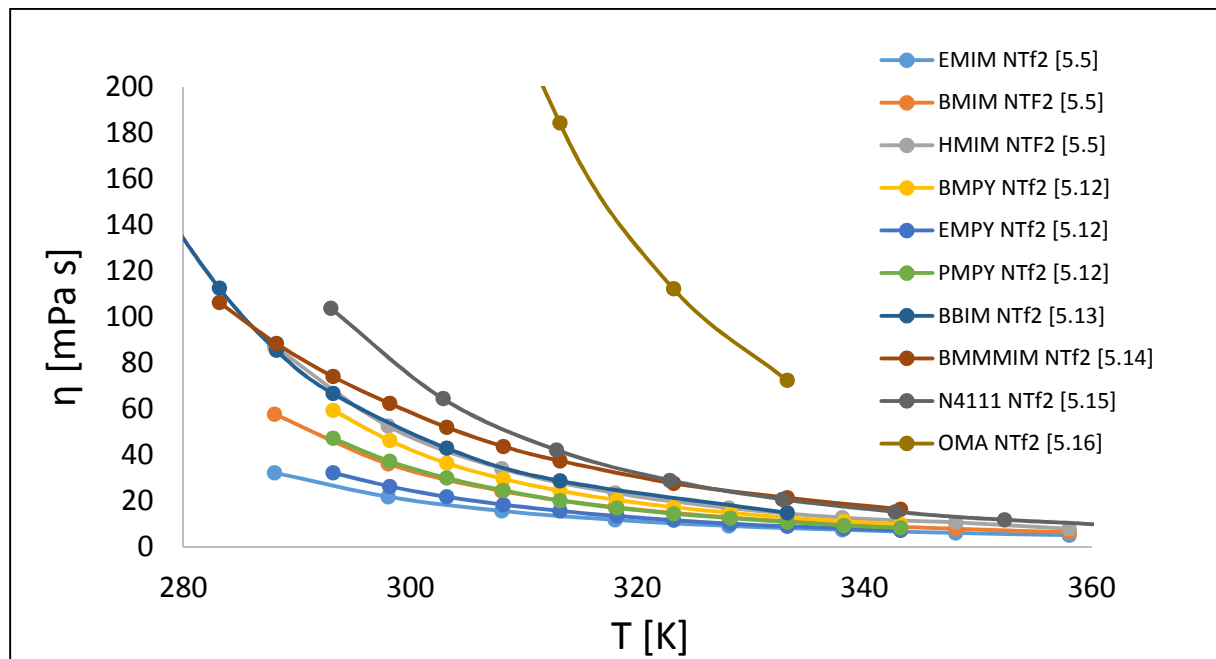


Figure 5-2: Temperature dependent dynamic viscosities of different NTF⁻-based ILs from literature

The references are mentioned in figure 5-2, the abbreviations are displayed in the following. All imidazole-based cations end on the suffix IM, pyridinium-based cations end on the suffix PY and all other cations here are ammonium-based. The letters before name the substituents: M for methyl, E for ethyl, P for propyl, B for butyl and H for hexyl respectively. The only exception is C4D since this cation has three substituents: one butyl and two methyl.

The advantage of the display in figure 5-2 is that one can upon extrapolating the experimental data easily read the theoretically accessible temperature window by drawing a horizontal line at a specific viscosity. The system with the largest temperature window was chosen.

The next step was to theoretically predict the temperature at which each mixture has a dynamic viscosity of 30 mPa s. The reason for this arises from an experimental consideration: Instead of characterizing the whole temperature region only a narrow temperature range around the desired value should be studied to minimize the experimental error on the slope in the relevant region.

Different models were applied to the problem and the best results were obtained by the empirical mass based Refutas equation which is displayed in equation 5.1. [5.17]

$$\nu_{mixture} = \exp\left(\exp\left(\frac{VBN_{mixture} - 10.975}{14.534}\right)\right) - 0.8 \quad (5.1)$$

It uses kinematic viscosities ν which are interconverted to dynamic viscosities η by division with the density ρ . $VBN_{mixture}$ denotes a so-called viscosity blending number which is calculated according to equation 5.2.

$$VBN_{mixture} = \sum_{i=0}^n x_i * VBN_i \quad (5.2)$$

Here VBN_i denotes the viscosity blending number of each individual component which is calculated from equation 5.3. We used literature values that correspond to our own measurements. [5.16]

$$VBN_i = 14.534 * \ln(\ln(\nu_i + 0.8)) + 10.975 \quad (5.3)$$

The final predictions of this method provided sufficiently good values with an average accuracy of ± 5 K compared to the experiment.

5.3 Experimental

ILs were purchased from Io-Li-Tec (Germany) and dried for 36 h at elevated temperature (40°C) and high vacuum. The process of drying can be monitored by NIR spectroscopy. After drying ILs were stored and handled under nitrogen atmosphere using Schlenk techniques.

It is important to mention that due to the IL's high viscosity the mass should be used instead of the volume to calculate concentrations and molar fractions. This reduces the error on the final concentration significantly. The overall volume of each mixture was less than 10 ml.

TTF (TCI >98 %) was purified by sublimation and used to synthesize $TTF^{\bullet+} ClO_4^-$ by the procedure of Hünig et al. [5.9] Both substances were stored in a desiccator over P_4O_{10} .

The samples were prepared from a stock solution of radical in order to ensure a constant concentration. This was necessary due to the relative small sample volumes (less than 0.5 ml) that were used. The final radical concentration was about 0.2 mM and the four additional samples contained neutral TTF up to 25 mM.

The ESR experiments were performed with the special flow systems for ILs described in chapter 4.4. Spectra were recorded with 100 kHz modulation and a modulation amplitude of 0.1 G. Each data point was repeated three times in order to ensure reproducibility.

5.4 Results and Discussion

The dependence of the density ρ on the temperature T was fitted by the linear approach given in equation 3.2. The coefficients a and b are listed in table 1. For the viscosities the simple Arrhenius-type equation 3.3 was used. Due to the small temperature window which is in the almost linear regime of the exponential this approximation is sufficient. The values for η_0 and H_η are also listed in table 5-1.

Table 5- 1: Experimental parameters to calculate density and dynamic viscosity

mixture	x(EMIM)	H_η [kJ mol ⁻¹]	η_0 [mPa s]	a [10 ⁻³ kg dm ⁻³ K ⁻¹]	b [kg dm ⁻³]	range T [K]
E100	1.00	26.91	-7.43	-1.02	1.821	290 - 310
E802	0.84	29.56	-7.81	-0.86	1.647	300 - 330
E505	0.56	34.11	-8.78	-0.81	1.489	310 - 345

Figure 5-3 displays the related experimental data for the values in table 5-1.

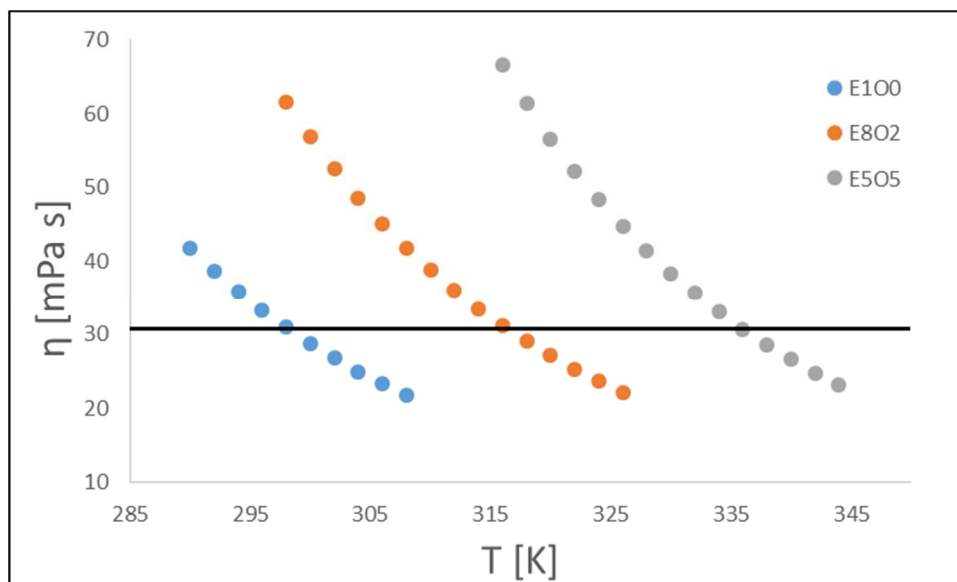


Figure 5-3: Experimental dynamic viscosities versus temperature

From this data the following temperatures were extracted for a constant viscosity: 298 K for E100. 316 K for E802 and 336 K for E505. It is visualized by the horizontal line. At these temperatures a line-broadening experiment was performed in the corresponding mixture.

In order to prove the principle only a simplex-algorithm in winsim2002 was used to extract the line-width ΔB_{pp} . Since the spectra are strongly asymmetrically broadened only the central line was considered. The result is displayed in figure 5-4 where the line widths are normalized to the one of the pure radical spectrum.

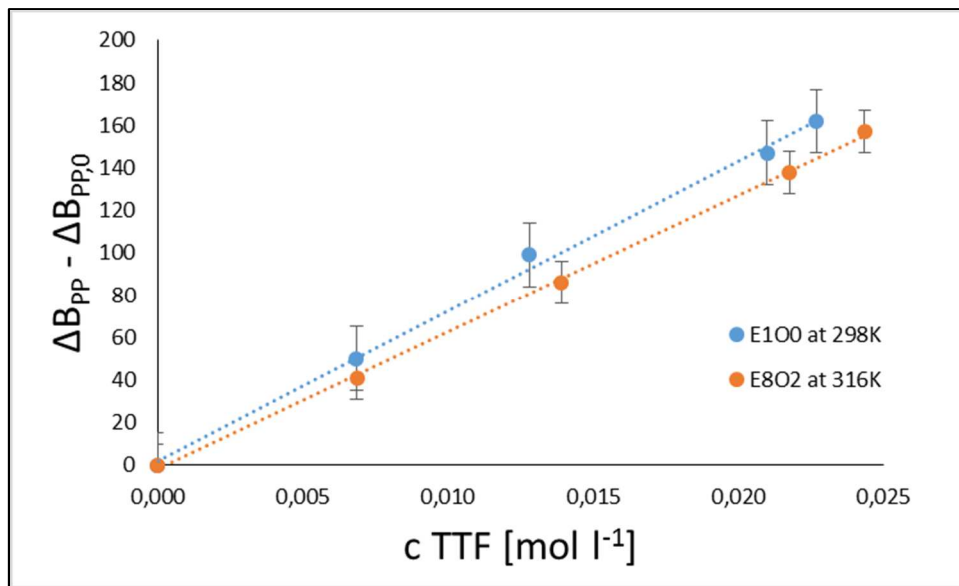


Figure 5-4: Plot of the normalized line width versus concentration of neutral TTF.

Unfortunately no data can be displayed for mixture E5O5. With an increasing molar fraction of OMA NTF₂ the substances are not completely soluble at room temperature. Therefore precipitation in our tubing led to non-systematic and irreproducible results.

For the remaining mixtures a rate was extracted under the assumption of slow exchange. The statistical factor p_i was set to $1/5$. This is valid since all five lines are baseline-separated. The rates are $1.35 \cdot 10^8 \text{ l mol}^{-1} \text{ s}^{-1}$ in E100 at 298 K and $1.23 \cdot 10^8 \text{ l mol}^{-1} \text{ s}^{-1}$ in E5O5. Within experimental error – which is estimated to be about 20 % for this method – they are basically the same. Comparing this to the theoretical rates of mass transport which are in between $2.2 \cdot 10^8 - 2.5 \cdot 10^8 \text{ l mol}^{-1} \text{ s}^{-1}$ the previous assumption of total diffusion control is valid. The rates of mass transport were calculated from the simplified Smoluchowski equation from chapter 1.6.

5.5 Conclusion and Outlook

The experimental approach to eliminate the temperature dependence of viscosity is conclusively shown to be operational. This leads to a significantly better control when studying any activated process in ILs since the data will correspond more exclusively to the process of interest due to a reduced bias from additional temperature dependent phenomena. Moreover, it is a new definite indication that macromolecular diffusion in ILs is really directly linkable to processes such as electron self-exchange on the microscopic scale which is usually just assumed throughout literature.

In the context of a master's thesis these results were successfully reproduced with a more systematic approach. The experimental issues were solved by applying the more time

intensive method of sealed samples which is described in chapter 4.2. The final results and conclusions have been published recently. [5.8]

5.6 References

- [5.1] P. Wasserscheid and T. Welton. *Ionic Liquids in Synthesis*. Wiley (2003)
- [5.2] N.V. Plechkova and K.R. Seddon. *Chem. Soc. Rev.* 37. 123 (2008)
- [5.3] Q. Li. J. Chen. L. Fan. X. Kong and Y. Lu; *Green Energy & Environment* 1. 18 (2016)
- [5.4] a) T.H.Y. Ha. K. Rasmussen. S. Langraf and G. Grampp. *Electrochim. Acta* 141. 72 (2014)
b) A. Patah. J. Bächle and G. Grampp. *Electrochim. Acta* 219. 305 (2016)
- [5.5] B. Sudy. PhD-thesis. Graz University of Technology (2015)
- [5.6] B. Sudy. K. Rasmussen and G. Grampp; *Mol. Phys.* 113. 1378 (2015)
- [5.7] B.Y. Mladenova. D.R. Kattinig. B. Sudy. P. Choto and G. Grampp; *Phys. Chem. Chem. Phys.* 18. 14442 (2016)
- [5.8] J. Bächle. M. Berghold. S. Landgraf and G. Grampp; *Chem. Phys. Chem.* (2017)
- [5.9] S. Hünig. G. Kießlich. H. Quast. and D. Scheutzow. *Liebigs; Ann. Chem.* 1973. 310 (1973)
- [5.10] T. L. Greaves. A. Weerawardena. C. Fong. I. Krodkiewska and C.J. Drummond; *J. Phys. Chem. B* 110. 22479 (2006)
- [5.11] A. Knorr and R. Ludwig; *Sci. Rep.* 5. 17505 (2015)
- [5.12] R.G. Seoane. S. Corderí. E. Gómez. N. Calvar. E.J. González. E.A. Maced and Á. Domínguez. *Ind. Eng. Chem. Res.* 51. 2492 (2010)
- [5.13] B. Hasse. J. Lehmann. D. Assenbaum. P. Wasserscheid. A. Leipertz and A. P. Fröba. *J. Chem. Eng. Data* 54. 2576 (2009)
- [5.14] O.O. Okoturo and T.J. VanderNoot. *J. Electroanal. Chem.* 568. 167 (2004)
- [5.15] J. Jacquemin. P. Husson. A. A. H. Padua and V. Majer. *Green Chem.* 8. 172 (2006)
- [5.16] A.P. Fröba. H. Kremer and A. Leipertz. 112. 12420 (2008)
- [5.17] Robert E. Maples. *Petroleum Refinery Process Economics*. 2nd Edition. Pennwell Books (2000)

6. Electron self-exchange of 9H-thioxanthen-9-one 10,10-dioxide and its corresponding radical anion

6.1 Introduction

In figure 6-1 the structure of 9H-thioxanthen-9-one 10,10-dioxide (TXO₂) is displayed. The electron self-exchange of sulfonic acid derivatives of anthraquinone and their semiquinone radicals have been subject to intense research in our group before. There the semiquinone radicals were produced photochemically. [6.1] More than a century ago it

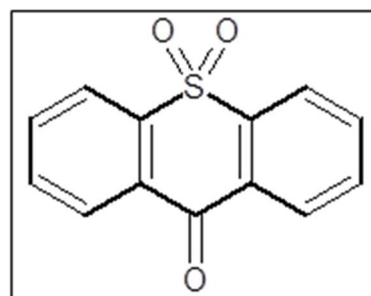


Figure 6-1: Structure of TXO₂

has been reported that TXO₂ changes its colour in alkaline alcohol in the presence of reducing agents such as zinc. [6.2] Various groups confirmed by ESR spectroscopy that this can be attributed to the formation of a ketyl type radical anion. [6.3] In terms of resonance structures the radical could be drawn at any position of the aromatic rings. This explains why it is relatively stable in solution even though atmospheric oxygen will oxidize it back to the ketone. This was used for educational purposes used in the way of a reverse blue-bottle experiment. [6.4]

Surprisingly no literature data on electron self-exchange kinetics of this system could be found. This might be related to the fact that in previous studies the radical was generated with zinc dust or molten alkali metals. This method was reproduced in the framework of a bachelor thesis. [6.5] With this methods the radical concentration cannot be controlled sufficiently. During some preliminary investigations it was found that the radical is formed either electrochemically or photochemically – even at ambient light with a couple of hours – in alkaline alcohol. Using the photochemical setup (see chapter 3.6) line broadening experiments on this system could readily be performed.

In the mixture of water/ethanol (3:7 vol.) the pH value can be controlled additionally. Theoretically it seemed possible to switch from electron self-exchange at high pH to proton coupled electron self-exchange at small pH upon protonating the alcohol type oxygen. Similar studies were performed on different types of quinones in order to differentiate between electron and proton transfer. [6.6] The TXO₂ system seemed more promising since the sulfonyl

group will not interfere by the means of an additional exchange process in contrast to the second alcohol function of a quinones. Unfortunately the TXO₂ radical anion is not stable at low pH-values.

6.2 Experimental

TXO₂ was synthesized from 2 g thioxantone (>98 % TCI) in 20 ml refluxing glacial acetic acid (100 % Merck) with 4ml of hydrogen peroxide (30 % Carl Roth) according to the procedure of Ullmann et al. [6.7] At room temperature it is a yellow suspension which turns into a deeply yellow solution close to the boiling point of the solvent. Within 2 h the solution bleaches constantly into a pale yellow. The product precipitates upon cooling to room temperature as yellow needles. Multiple recrystallization cycles from 60 ml refluxing ethanol (99.9 % AustrAlco) white needles can be obtained. The melting point was 186 – 187 °C which corresponds to literature.

For this system samples of at least 50 ml per measurement were prepared in at ambient atmosphere from two stock solutions per sample. Solution A are different concentrations of TXO₂ dissolved in ethanol (99.9 % AustrAlco) with an ultrasonic bath. The concentrations of TXO₂ usually range from 0.5 mM to 5 mM for each line broadening experiment. Solution B is a buffer with a defined pH in water. (bidest) pH > 12 was realized with different concentrations of pure NaOH (>99% Baker) at pH > 12, for 12 > pH > 8 a carbonate buffer was used and for smaller pH a glycine buffer. The usual ratio of A/B was 7/3 and the final buffer concentration 0.1 M.

A constant radical concentration was produced in the photochemical flow system (chapter 4) upon varying the flow rate. Depending on the amount of TXO₂ they ranged from 2 ml min⁻¹ to 20 ml min⁻¹. All spectra were recorded at 293 K with a 0.1 G modulation amplitude. The concentration was checked via double integral where an error of 5 % was tolerated. In order to ensure reproducibility each sample was prepared and measured three times.

6.3 Results and Discussion

Two exemplary spectra – one of the pure radical and one with additional neutral TXO₂ – and the corresponding simulations are displayed in figure 6-2.

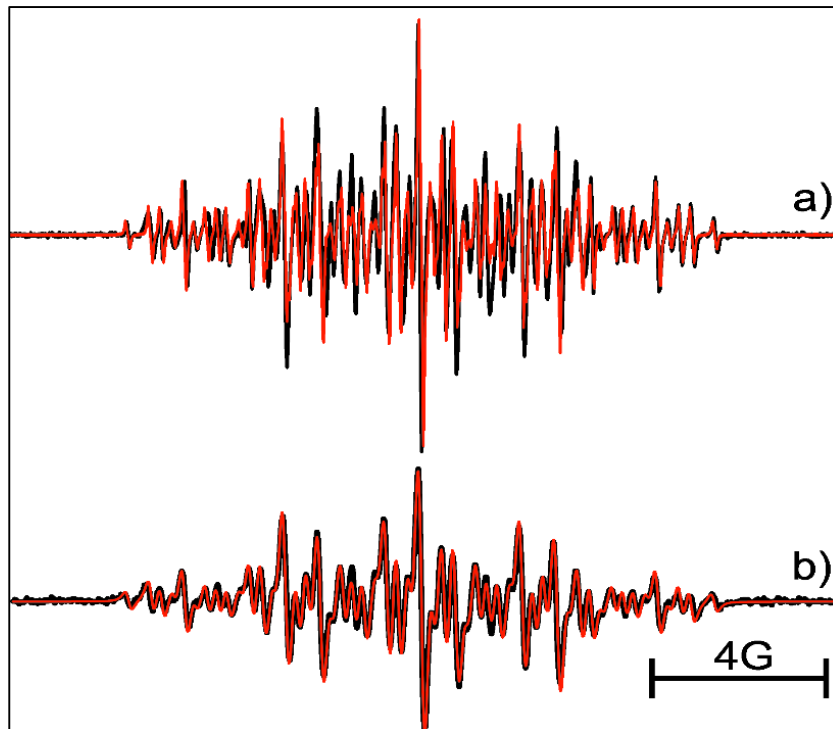


Figure 6-2: Spectra of a) 0.5 mM photo-generated TXO₂^{•-} in ethanol/water (7:3 vol.) at pH 13 and b) with 5 mM neutral TXO₂

Due to the four sets of hydrogen atoms the spectra are relatively complicated but quite well resolved. The corresponding hyperfine splitting constants: a_1^{2H} 3.18 G, a_2^{2H} 2.33 G, a_3^{2H} 0.78 G and a_4^{2H} 0.53 G were used in order to fit the experimental spectra. They are similar to the ones from literature, which were used as initial starting values for the simulations. There they have additionally be assigned as displayed in figure 6-3. [6.3]

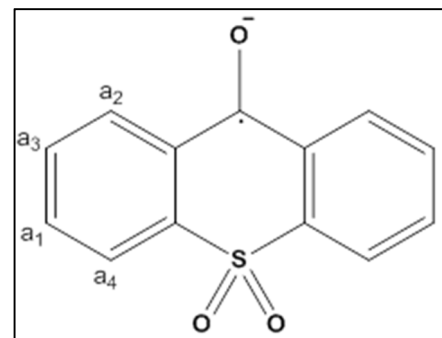


Figure 6-3: assignment of the hyperfine splitting constants

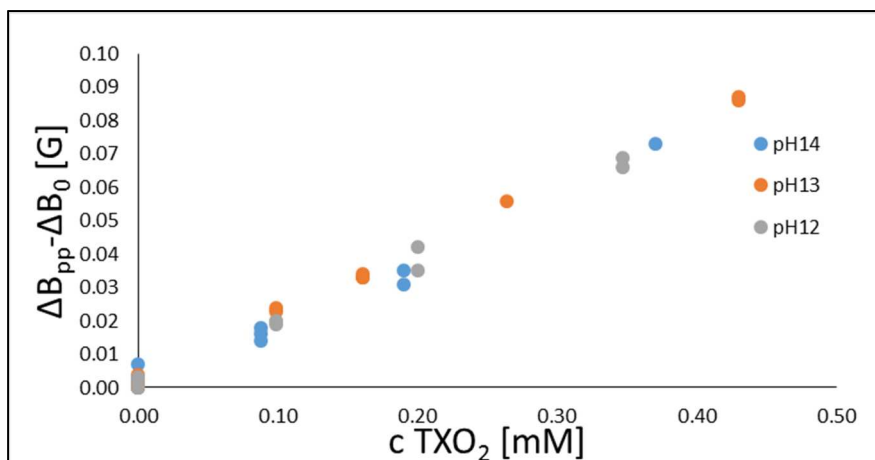


Figure 6-4: Data points of line broadening experiments at different pH

The data points from line broadening experiments at different accessible pH values are overlaid in figure 6-4. The offset on y-axis is related to varying concentrations of radical for individual experiments.

From the linear regression of the data in figure 6-4 a rate k_{obs} was extracted under the assumption of slow exchange according to equation 2.59 in Chapter 2.6. Due to the multitude of lines in the spectrum the statistical factor p_i is expected to be small. Therefore this correction is negligible so that the value of p_i was set to zero. In order to obtain an electron self-exchange rate k_{ET} the diffusion correction according to equation 2.66 in chapter 2.6 was applied. The value of $\eta = 2.447 \text{ mPa s}$ was used to calculate k_{diff} was taken from literature. [6.8]

Table 6-1: Experimental and calculated rates in $M^{-1} s^{-1}$

Sample	k_{obs}	k_{diff}	k_{ET}
pH 14	2.80E+08	2.63E+09	3.55E+08
pH 13	3.00E+08		3.89E+08
PH 12	2.89E+08		3.70E+08

The values of k_{ET} are relatively slow which is not surprising for this relatively large molecule. Further they do not change within experimental error – it was estimated to be about 10 % – with the pH value. This is expected since protonation occurs at lower pH values.

Decreasing the pH value in the mixture revealed two important features of this system. Firstly the radical is not produced in the absence of OH^- ions which limits the available buffer systems to $\text{pH} > 8$. Secondly it was observed that the radical immediately disappears if the pH value is lowered below pH 8 upon adding mild acids. However, it reappears upon increasing the pH again. This behaviour is attributed to a reversible dimerization of the radicals in one of the many mesomerically accessible aromatic positions. At high pH the columbic repulsion keeps the radical anions separated. Protonation, however, leads to electrically neutral radicals that can dimerize. These protonation and deprotonation cycles and subsequent reversible dimerization can be repeated multiple times without losing radicals.

Moreover, the possibility to study the system in other solvents that are miscible with water was explored. This criteria was chosen since our focus was on pH depended experiment which require to dissolve a buffer. Linear alcohols up to butan-1-ol give nice and comparable spectra but were not investigated further.

6.4 Outlook and Conclusion

Electron self-exchange rates of the $\text{TXO}_2/\text{TXO}_2^{\bullet-}$ system were measured by ESR line broadening experiments for the first time. This could be achieved by the alternative photochemical radical generation in our flow system.

However, the theoretical switch from electron to proton coupled electron transfer by control of the pH value is not possible due to reversible dimerization. This intrinsic chemical reactivity might be overcome by steric substituents which most likely display disadvantageous solubility and even more complicated ESR spectra. In the accessible pH range no effect on the exchange-kinetics was observed.

For future work which was not of interest in the course of this thesis it could be an interesting system to study the electron self-exchange in dependence of temperature and solvents. Since this system is soluble in alcohols it could additionally be used to gain additional knowledge on solvent dynamics in non-Debye solvents. [6.9] This topic was addressed in our group before. [6.10]

6.5 References

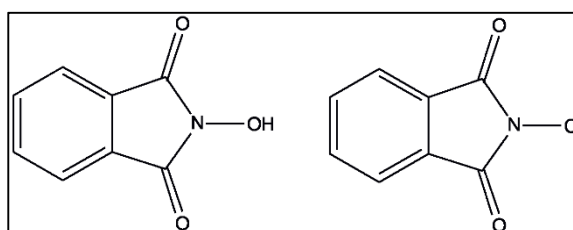
- [6.1] B. Mladenova, PhD-Thesis, Graz University of Technology (2006)
- [6.2] C. Gräbe and O. Schlutess, *Ann.* 263, 11 (1891)
- [6.3] a) M. M. Urberg and E.T. Kaiser, *J. Am. Chem. Soc.* 89, 5179 (1967)
b) T. Aruga, O. Ito and M. Matsuda, *J. Am. Chem. Soc.* 101, 7585 (1979)
- [6.4] J. Castrillón, *J. Chem. Ed.* 64, 352 (1987)
- [6.5] P. L. M. L. Riedl, Bachelor Thesis, Graz University of Technology (2016)
- [6.6] G. Grampp and W. Jaenicke, *J. Electroanal. Chem.* 229, 297 (1987)
- [6.7] F. Ullmann and O. von Glanck, *Be.* 19, 2487 (1916)
- [6.8] R. Bela, J.V. Herraiez and O. Diez, *Phys. Chem. Liq.* 42, 467 (2004)
- [6.9] A. V. Barzykin, P. A. Frantsuzov, K. Seki and M. Tachiya, *Adv. Chem. Phys.* 123, 511 (2002)
- [6.10] P. Choto, K. Rasmussen and G. Grampp, *Phys. Chem. Chem. Phys.* 17, 3415 (2015)

7. Hydrogen atom self-exchange of NHPI/PINO

7.1 Introduction

When this project started no report on ESR line-broadening experiments for intermolecular hydrogen atom self-exchange could be found even though there are organic radicals that react within the experimental time resolution. The literature so far focused exclusively on comparably slow reactions of metalorganic complexes since the rates of these systems are accessible to NMR line broadening experiments. [7.1]

In literature N-hydroxyphthalimide (NHPI) is well established as organo-catalyst for selective oxidation reactions of hydrocarbons and widely exploited in industry accordingly.



Current literature is consistent that the initial

Figure 7-1: Structures of NHPI (left) and PINO (right)

step of the catalytic process is the generation of a phthalimide-N-oxyl radical (PINO) which then abstracts a hydrogen atom from the substrate. [7.2] Figure 7-1 displays the corresponding structures.

The reactivity towards different substrates has been studied extensively for the last decades which also involves the study of kinetics. Since the reactions are rather fast the scope of methods with an appropriate time resolution such as Rotating Disk Electrode Voltammetry, [7.3] Laser Flash Photolysis [7.4] or stopped-flow UV-VIS spectroscopy [7.5] is limited. Moreover, there were already first attempts towards the study of self-exchange by studying so-called pseudo self-exchange kinetics of reactions with an almost zero driving force. [7.6] In this work the authors reasoned quite conclusively that this system reacts via a for organic radicals typical HAT pathway which was adopted for this interpretation.

All the studies on NHPI reported hydrogen abstraction rates in the order of $10^8 \text{ M}^{-1} \text{ s}^{-1}$ which is conveniently within the time resolution of ESR line broadening experiments. The generation of PINO is rather straight forward since it is available through chemical, electrochemical and photochemical methods. Unfortunately the radical decomposes within minutes which was studied in detail before. [7.7]

This problem was overcome by using an electrochemical flow system. In order to really observe the simple HAT process only in different aprotic media were used as solvent. This

circumvents the potential interference of additional protonation equilibria with the anionic species of NHPI. The experimental data correlates with to the dynamic viscosity which could be explained theoretically.

7.2 Experimental

The commercial NHPI (Sigma Aldrich 98 %) was recrystallized from hot distilled water, which yields long yellow needles. These needles start to decompose at about 506 K according to literature. [7.8] In order to keep them dry they were stored over P_4O_{10} under reduced pressure.

The supporting electrolyte tetrabutylammonium tetrafluoroborate (Fluka pure) was dried at 350 K under vacuum for at least 12 h and stored under nitrogen atmosphere.

All solvents – acetone, (Ac_2O) acetonitrile, (MeCN) propionitrile, (EtCN) nitromethane, ($MeNO_2$) dimethyl sulfoxide (DMSO) and propylene carbonate (PC) – were dried and purified as described in chapter 4.1.

Solutions of 0.1 M supporting electrolyte were characterized in terms of dynamic viscosity by the methods described in chapter 4.6 at 295 K.

Samples were prepared in a Schlenk system from a degassed solvent stock containing 0.1 M supporting electrolyte. This stock solutions were characterized as described in chapter 4.6 since the viscosity is dependent on the supporting electrolyte. [7.9] From the stock solutions about five samples of 10 – 15 ml each was prepared with a concentration $5 * 10^{-4} - 2 * 10^{-2}$ M NHPI. In Acetonitrile the solubility is worse, therefore the concentration range is limited up to a maximum of $1.5 * 10^{-2}$ M.

For each solvent the flow rate (usually around 0.5 ml min^{-1}) and exchange current was optimized in the electrochemical flow system (see chapter 3.5) to the maximal integral of the lowest concentration of NHPI. For the analysis quantitative electrochemical conversion was assumed. About 10 spectra per sample were recorded with 100 kHz modulation and a modulation amplitude of 0.5 G. The final radical concentration was checked by double integration. Due to the low noise deviations on this quantity are below 5 %.

7.3 Results and Discussion

The ESR spectrum of PINO is described in literature. [7.10] Two triplets arising from the interactions with 1N and 2H dominate the spectrum. From the structure one would expect an additional hyperfine splitting from the second set of protons, however, it is too small to be

observed experimentally up to now. Due to the limited stability there is also no data from ENDOR experiments available.

In the more viscous solvents DMSO and PC additional inhomogeneous broadening was observed from rotational anisotropy. Comparing the low to the high field lines the difference in line width is about 50 mG at room temperature. Figure 7-2

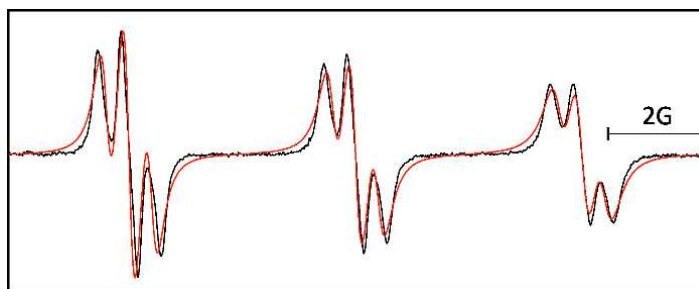


Figure 7-2: ESR spectrum of 0.5 mM electro-generated PINO in PC at 295 K with 0.1 M TBA BF₄ (black) and corresponding simulation (red)

displays an exemplary spectrum with a crude corresponding simulation. For the later analysis each line was analysed individually for this type of spectrum – which only occurs in high viscous solvents – since the applied simulation routine did not attribute for this effect. This explains the obviously poor line-shape displayed in figure 7-2 for the overall spectrum.

In figure 7-3 an exemplary line broadening experiment with corresponding simulations is displayed. The correlation is despite the already mentioned missing hyperfine splitting constant more than sufficient for the homogeneous broadened spectra in low viscous solvents.

The hyperfine splitting constants used in the simulations were extracted from the standard ESR spectra by standard fitting routines and are listed in table 7-3. They are not strongly dependent on the solvent.

The broadening was interpreted by equation 2.59 as described in chapter 2.6 under the assumption of slow exchange. This is reasonable due to the low concentrations and the dominant nitrogen coupling which remains base line separated up to slightly below the highest concentration. Due to this dominant coupling the statistical factor p_i was estimated to be 1/3. Related plots are displayed in figures 7-4 and 7-5.

Table 7-1: Experimental hyperfine splitting constants

solvent	a^{1N} [G]	a^{2H} [G]
Ac ₂ O	4.72	0.44
DMSO	5.04	0.46
EtCN	4.78	0.47
MeCN	4.77	0.46
MeNO ₂	4.83	0.49
PC	4.85	0.48

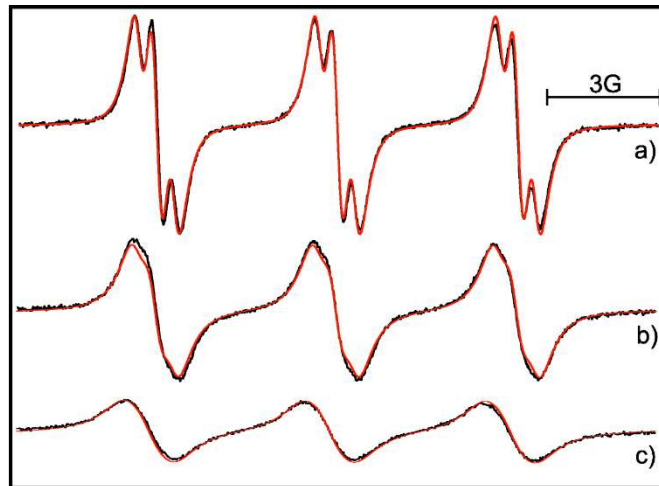


Figure 7-3: ESR spectra (black) of (a) 0.5 mM electro-generated PINO in MeCN at 295 K with 0.1 M NaClO₄ (b) with 10 eq. NHPI and (c) with 20 eq. NHPI and corresponding simulations (red)

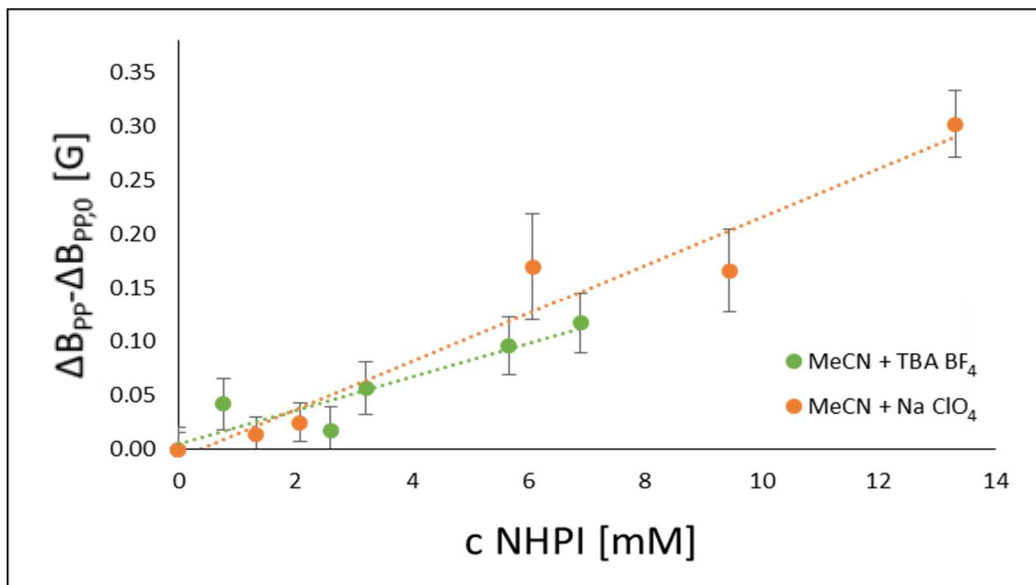


Figure 7-4: Plot of additional line broadening versus concentration of NHPI in different solvents with 0.1 M of TBA BF₄

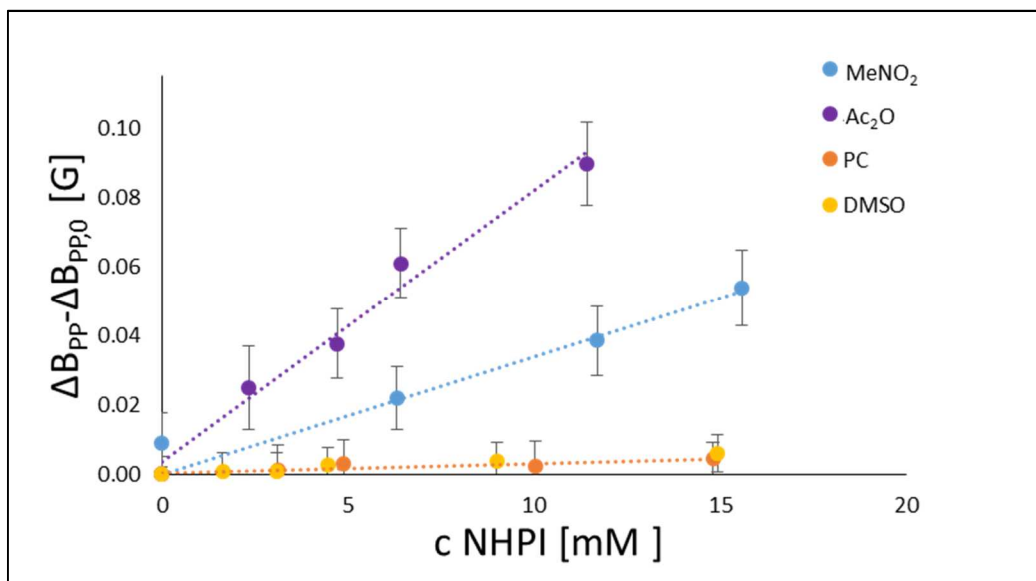


Figure 7-5: Plot of additional line broadening versus concentration of NHPI in MeCN with different supporting electrolytes

All experimental rates k_{obs} are listed in table 7-2. Additionally experimental values for the density ρ and the kinematic viscosity ν are mentioned. From those the dynamic viscosity η was calculated as the quotient ρ/ν . These values were used to determine k_{diff} for the diffusion correction by equation 2.64 in chapter 2 in order to determine the hydrogen atom self-exchange rate k_{H} . Note that all rates are expressed in the order of $10^{-8} \text{ M}^{-1} \text{ s}^{-1}$.

Table 7-2: Experimental rates in $10^{-8} \text{ M}^{-1} \text{ s}^{-1}$ and solvent parameter

solvent	k_{obs}	k_{diff}	k_{H}	$\rho [\text{g ml}^{-1}]$	$\nu [\text{mm}^2 \text{ s}^{-1}]$	$\eta [\text{Pa s}]$
MeCN + Na ClO ₄	5.69	173	6.09	0.7857	0.48	0.38
MeCN + TBA BF ₄	3.53	153	3.70	0.7512	0.57	0.43
A ₂ O + TBA BF ₄	1.80	187	1.84	0.7926	0.44	0.35
MeNO ₂ + TBA BF ₄	0.64	158	0.65	1.1280	0.60	0.42
DMSO + TBA BF ₄	0.09	29.7	0.09	1.0938	2.01	2.20
PC + TBA BF ₄	0.06	23.5	0.06	1.1966	2.33	2.79

The overall error on these rates was estimated to be about $\pm 10\%$. The main source of error is related to the radical concentration which was addressed in chapter 4.5.

The fact that the rates differ over two orders of magnitude emphasises strong solvent effects which were discussed in chapter 1. The most reasonable correlation of k_{H} with a solvent property was found for the dynamic viscosity. Figure 7-6 displays a Kramer type plot of the experimental data.

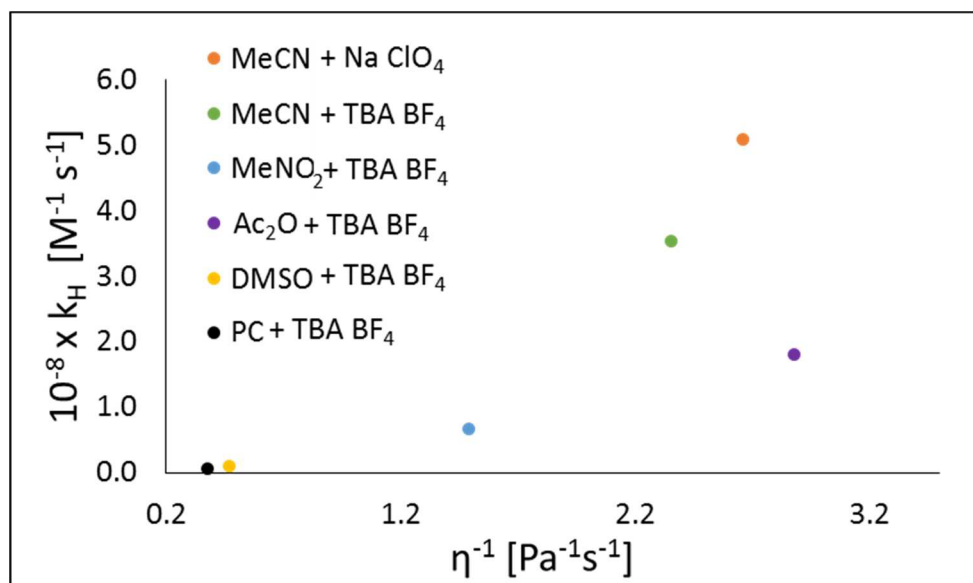


Figure 7-6: Kramer type plot of k_{H} versus η^{-1}

The linear relation from Kramer theory is observed for all solvents except MeCN. We interpret this deviation in the framework of an expanded Kramer type theory. Standard Kramer theory relates the preexponential factor to η^{-1} . It treats the reorganization of the medium which has to correspond to the change of volume and shape of the reactants inside a reaction cage in terms of statistical dynamics. An additional term is introduced to the preexponential factor.

This term is related to interactions of the solvent. [7.11] These interactions are significantly different in the more Lewis basic nitrile. Therefore experiments in different nitriles were tested, however, in propionitrile an insufficient signal to noise ratio was obtained. In butyronitrile and benzonitrile no ESR signal was observed at all as well as in tetrahydrofuran and dimethylformamide.

The rate k_H in MeCN is dependent on the dynamic viscosity nonetheless. This was demonstrated upon changing to a smaller supporting electrolyte. Since the viscosity can be interpreted as an activated process of changing the location the smaller supporting electrolyte obstructs the motion less. Therefore the dynamic viscosity decreases and k_H increases respectively. Additionally a bigger tetraoctyl-ammonium based supporting electrolyte was tested but the measured increase of the dynamic viscosity was too small. Alternatively the viscosity could be influenced by the electrolyte concentration according to the Jones-Dole equation. [7.12] This is not favourable in terms of a reproducible electro-chemical conversion and comparably small within the limitations of solubility.

7.4 Outlook and Conclusion

Within this project the first application of the ESR line broadening experiment to the process of hydrogen atom self-exchange was demonstrated. The main advantage is that the superior time resolution enables to investigate reactive and therefore fast systems. Since organic radicals play a major role in current applications such as industrial organo catalysis the limitations of ESR spectroscopy are perfectly circumvented.

This study we explores the possibilities within the limitations of the current equipment. For future work it will be essential to implement a way to control the temperature in order to obtain thermodynamic parameters. These are key to really understand the physics behind the theoretical parameters from the expanded Kramer theory that was employed.

Further the NHPI/PINO system is limited by its stability as well as its solubility. Therefore this experiments have to be expanded to other systems which are more stable and soluble in a larger variety of solvents. In the course of our work a variety of systems were examined. Firstly derivatives of 2,2,6,6-tetramethylpiperidine-1-oxyl and the corresponding hydroxyl amines were finally ruled out since they are not stable enough. Secondly, substituted triphenyl ammonium salts and the corresponding radical cations were excluded since they have rather complicated spectra with poor resolution which doesn't allow proper analysis. Thirdly a phenole/phenoxyl couple was investigated which is discussed in chapter 8.

Finally it would be interesting to study systems that are soluble in water or other protic solvents in order to access different types of proton coupled electron transfer by changing the pH value e.g. in chapter 6 this topic has already been addressed.

7.5 References

- [7.1] a) J.D. Protasiwicz and K.H. Theopold, *J. Am. Chem. Soc.* 115, 5559 (1993)
b) J.D. Soper and J.M. Mayer, *J. Am. Chem. Soc.* 125, 12217 (2003)
- [7.2] a) F. Recupero and C. Punta, *Chem. Rev.* 107, 3800 (2007)
b) S. Coseri, *Cat. Rev. – Sci. Eng.* 51, 218 (2009)
- [7.3] S. Kishioka and A. Yamada, *J. Electroanal. Chem.* 578, 71 (2005)
- [7.4] a) E. Baciocchi, M. Bietti, M.F. Gerini and O. Lanzalunga, *J. Org. Chem.* 70, 5144 (2005)
b) D. Alfonso, M. Bietti, G.A. DiLabio, O. Lanzalunga and M. Salmone, *J. Org. Chem.* 78, 1026 (2013)
- [7.5] N. Koshino, Y. Cai and J.H. Espenson, *J. Phys. Chem. A* 107, 4262 (2003)
- [7.6] Y. Cai, N. Koshino, B. Saha and J.H. Espenson, *J. Org. Chem.* 70, 238 (2005)
- [7.7] C. Ueda, M. Noyama, H. Ohmori and M. Masui, *Chem. Pharm. Bull.* 35, 1372 (1986)
- [7.8] D.E. Ames and T.F. Grey, *J. Chem. Soc.* 1955, 3518 (1955)
- [7.9] G. Jones and M. Dole, *J. Am. Chem. Soc.* 51, 2950 (1929)
- [7.10] H. Lemaire and A. Rassat, *Tetrahedron Lett.* 33, 2245 (1964)
- [7.11] I. V. Aleksandrov and V. I. Gol'danskii, *Chem. Phys.* 87, 455 (1984)
- [7.12] G. Jones and M. Dole, *J. Am. Chem. Soc.* 51, 2950 (1929)
- [7.13] J. Bächle, F. Goni and G. Grampp, *Phys. Chem. Chem. Phys.* 17, 27204 (2015)

8. Hydrogen atom transfer dynamics in a hydrogen bonded complex of the Blue Aroxyl and the corresponding Phenol

8.1 Introduction

Especially in the field of biochemistry the conversion of a phenol to its corresponding phenoxyl radical plays an important role. Various antioxidants such as tocopherol (Vitamin E) [8.1] rely on this chemical transformation. Moreover, it occurs in the oxidation of tyrosine in Photosystem II which is followed by a fast proton transfer to a hydrogen bonded histidine [8.2] or the reduction of ribonucleotides. [8.3]

The simplest model system would be the unsubstituted phenol. The corresponding radical is stabilized mesomerically but unfortunately prone to rapid dimerization. [8.4] Therefore the corresponding self-exchange reaction is only subject theoretical studies so far. These provided convincing evidence that the phenol/phenolate couple reacts via a PCET mechanism instead of the usually favoured HAT mechanism. [8.5]

The blue aroxyl derivative – 2,4,6-tri-*t*-butyl-phenoxy radical – is stabilized additionally by steric protection. The structure is displayed in figure 8-1. On the other hand this leads to considerably slow hydrogen atom exchange reaction rates which are accessible by NMR line broadening experiments. The first report estimates the hydrogen atom self-exchange rate of this system to be $300 \text{ M}^{-1} \text{ s}^{-1}$ at 303 K in carbon tetrachloride with a small activation energy of 1 kJ mol^{-1} . [8.6] This rate is

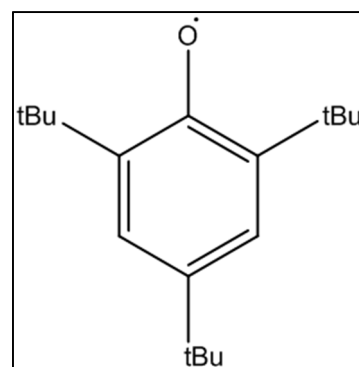


Figure 8-1: Structure of the blue aroxyl

comparable to more recent studies. A combination of NMR line broadening experiments on self-exchange and optical stopped flow methods on pseudo self-exchange to 2-methyl-4,6-dibutyl-phenol explained these rates conclusively in the context of bond dissociation enthalpies. [8.7] Additionally an ESR observation of the same pseudo-self-exchange reports a rate of $10^{10} \text{ M}^{-1} \text{ s}^{-1}$ in benzene/toluene 1/1 at 298 K. This value would exceed the limit of diffusion and appears therefore not to be trustworthy. [8.8]

These rates are too slow to be detected by the concentration dependent ESR line broadening experiment. However, changing the temperature in presence of excessive neutral phenol yields an alternating line width effect. This effect is discussed in chapter 2.6. It arises from a dynamic motion of the hydrogen atom in between the two oxygen atoms inside a hydrogen bonded complex which modulates the hyperfine couplings of the radical. From the experimental exchange frequencies activation energies and tunnelling contributions were found and interpreted by the Bell-Limbach theory. [8.9]

8.2 Experimental

The 2,4,6-tri-t-butyl phenoxy radical was synthesized from 2,4,6 tri t-butyl phenol (98% Aldrich). Careful consecutive sublimation and recrystallization from n-hexane yields a white instead of yellow starting material.

For the oxidation to the radical literature procedures were applied. [8.10] All steps were performed in Schlenk system in order to ensure an oxygen free Argon atmosphere. First 300 mg Potassium hydroxide and 2 g Potassium ferricyanide were completely dissolved in 7.5 ml of distilled water. Then 37.5 ml benzene were added and the solvents were purged with Argon for 1.5 h. Upon adding 500 mg of the phenol the solution changed almost instantly to a dark blue colour. Stirring was continued for 2 h before the aqueous layer was removed. The organic layer was dried with potassium carbonate for approximately 20 min. After a final filtration step the benzene was removed. Deep blue radical crystals remained which were dried carefully under high vacuum. When the crystals are dried and stored under Argon atmosphere the radical remains usable for 5 days before it starts to degrade. This is easily visible since the colour starts fading and eventually turns into green.

All solvents for sample preparation were dried by corresponding molecular sieves, distilled and degassed by bubbling dry nitrogen through prior to use.

The sealed ESR samples were prepared by the method described in chapter 3.2. For an experiment in one specific solvent two samples are required. Both have the same radical concentration of about 1 mM but one contains 100 mM of additional phenol.

The spectra were recorded with the standard equipment at X-Band with 100 KHz modulation with an amplitude of 0.1 G in temperature steps of 10 K. In order to ensure that a thermal equilibrium is established at every measurement point the temperature was held constant for 5 min prior to recording the spectrum.

8.3 Results and Discussion

The spectrum of the radical is well described in literature and even ENDOR spectra are available. [8.11] Additional weak signals of a second radical were observed at lower temperature since the natural line-width is small there.

Figure 8-2 displays a cut out of the relevant spectral region. We could

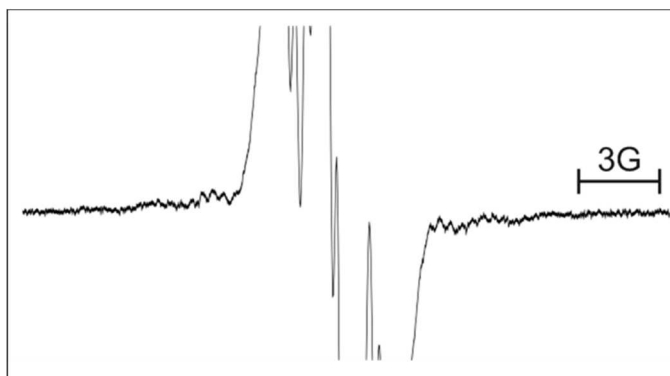


Figure 8-2: Zoom on the additional signals in an ESR spectrum of 0.1 M blue aroxyl in CS₂ at 240 K

attribute them to remaining 2,6-di-t-butyl-phenol by using literature values for the relevant hyperfine splitting constants – $a^{1H,p} = 9.63$ G and $a^{2H,m} = 1.96$ G – from literature [8-12] with an additional $a^{18H} = 0.4$ G from our spectra. It is an intermediate in the synthesis that cannot be absolutely removed. The same signal appears in highly resolved spectra but is not discussed in the related literature. [8-13] In order to exclude interference from this species with the experiments the content of this impurity was quantified by HPLC-MS. It is about 1% besides additional 2% of the potassium adduct of the 2,4,6-tri-t-butyl-phenol.

Figure 8-3 displays a set of ESR spectra of the blue aroxyl at different temperatures in carbon disulfide. From the significant broadening at low temperature it is obvious that the choice of the proper temperature range is crucial for this experiment. The main indications are the Curie behaviour of the signal intensity and the plots of

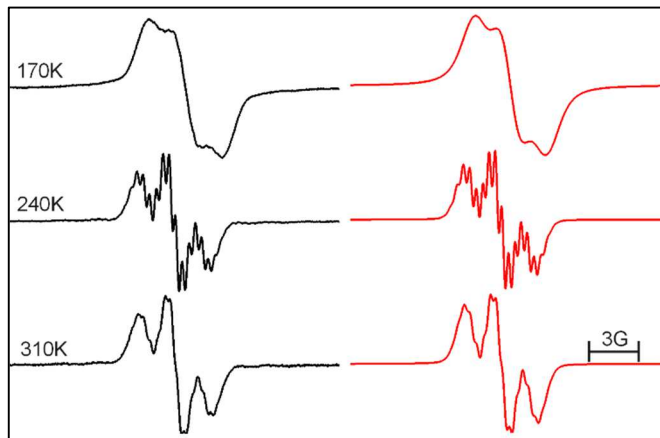


Figure 8-3: ESR spectra of 0.1 M blue aroxyl in CS₂ at various temperatures

Kivelson and Berner. Both methods are described in chapter 2.6 and yielded accessible temperature range in-between 220 K and 320 K.

Under the assumption of slow exchange we used the generalized Bloch formalism to interpret the broadening at each temperature relative to the pure radical spectrum. The resulting frequencies range from $10^4 - 10^6$ s⁻¹.

The resulting bend Arrhenius plots were simulated and interpreted reasonably with a program based on the theory of Bell and Limbach. [8.14] In order to do these simulations the logarithm of the preexponential factor was set to 12.6 since the contribution of the

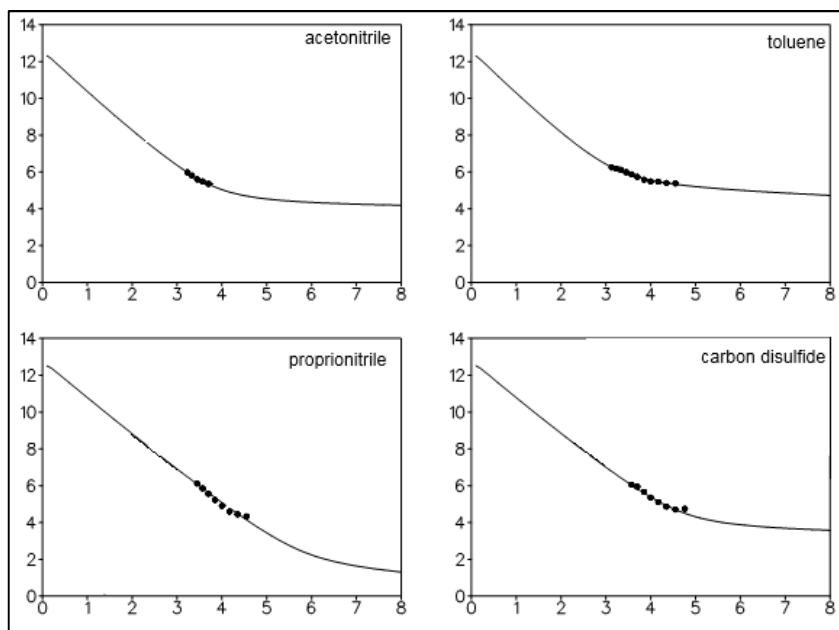


Figure 8-2: Experimental data and simulations as plot of $\log k$ versus T^{-1}

entropy was estimated to be small. The data is displayed in figure 8-3 and the activation parameters are listed in table 8-1. Here E_d denotes the activation barrier at high temperature, E_m the minimal tunnelling barrier, $2a$ the barrier width and Δm the effective tunnelling mass which considers heavy atom motion prior to tunnelling. This Δm is derived from the sum over all products from the mass of the heavy atom with the quotient of its displacement over the displacement of the tunnelling particle.

Table 8-1: Data simulated by the theory of Bell and Limbach

solvent	T range [K]	E_d [kJ mol ⁻¹]	E_m [kJ mol ⁻¹]	$2a$ [Å]	Δm [a.u.]
acetoneitrile	260 - 310	43.5	0.04	0.50	2.00
propionitrile	220 - 320	36.4	2.51	0.60	3.00
carbon disulfide	220 - 280	38.9	0.29	0.50	3.00
toluene	220 - 310	43.9	1.67	0.52	2.00

Even though it has to be considered that the temperature windows are small and the experimental error was estimated to be about 20 % this data shows a few interesting trends. First of all the activation energy does not change significantly with the solvent which supports the assumption of the permanent formation of hydrogen bonded complexes. Moreover, the remaining E_m in toluene suggests a parallel heavy atom motion of the oxygen atoms towards each other during the transfer which is supported by values for $\Delta m > 1$. In the other solvents the bend region is not accessible by this experiment, however, it is reasonable to assume the same mechanism. It is, however, important to consider that the Bell-Limbach model has been developed as a quick qualitative interpretation tool for experimental data.

8.4 Conclusion

This work shows that dynamic ESR is applicable to slow HAT processes as well, whereas the observed dynamic differs from the one discussed in chapter 7. Combining these two types of line broadening experiments dynamic ESR spectroscopy has the unique ability to access the whole kinetic range of hydrogen atom transfer for organic radicals.

Within a co-operation with Prof. Anne-Marie Kelterer (Graz University of Technology) and PhD Marijana Marković (Institute for Medical Research and Occupational Health Zagreb) this process was modelled by DFT and CASSCF calculations, which correspond to our experimental findings. The activation barriers are in the same order of magnitude and a relaxed scan reaction path modelling indicates the heavy atom motion during the transfer as well.

8.5 References

- [8.1] G.W. Burton and K.U. Ingold, *Acc. Chem. Res.* 19, 194 (1986)
- [8.2] B.A Diner, D.A. Force, D.W. Randall and R.D. Britt, *Biochemistry* 37, 17931, (1998)
- [8.3] M. Sjödin, S. Styring, B. Åkermark, L. Sun and L. Hammarström, *J. Am. Chem. Soc.* 122, 3932 (2000)
- [8.4] D.C. Nonhebel and J.C. Walton, *Free Radical Chemistry - Structure and Mechanism*, Cambridge University Press, Cambridge (1974)
- [8.5] a) J.M. Mayer, D.A. Hrovat, J.L. Thomas and W.T. Borden, *J. Am. Chem. Soc.* 124, 11142 (2002)
b) T. Inagaki, T Yamamoto and S Kato, *J. Comput. Chem.* 32, 3081 (2011)
- [8.6] R.W. Kreilick and S.I. Weißmann, *J. Am. Chem. Soc.* 84, 306 (1961)
- [8.7] J.J. Warren and J. M. Mayer, *Proc. Natl. Acad. Sci.* 107, 5282 (2010)
- [8.8] M.E. Coronel, *J. Int. J. Chem. Kinet.* 37, 1 (2005)
- [8.9] H.H. Limbach, J.M. Lopez and A. Kohen, *Phil. Trans. R. Soc. B* 361, 1399 (2006)
- [8.10] C.D. Cook and R.C. Woodworth, *J. Am. Chem. Soc.* 75, 6242 (1953)
- [8.11] E. Müller, *Rev. Port. Quím* 14, 129 (1972)
- [8.12] a) J. Pannel, *Chem. Ind. (London)*, 1797 (1962)
b) W.G.B. Huysmans and W. A. Waters, *J. Chem. Soc. B* 1047 (1966)
c) S.A. Weiner, *J. Am. Chem. Soc.* 94, 581 (1972)
- [8.13] K. Scheffler, *Z. Elektrochem.* 65 ,439 (1961)
- [8.14] J.M. López del Amo, PhD-Thesis, Freie Universität Berlin (2006)